Supplementary Information

Bifunctional Janus Particles as Multivalent Synthetic Nanoparticle-Antibodies (SNAbs) for Selective Depletion of Target Cells

Jiaying Liu,[1] Randall Toy,[*1] Casey Vantucci,[*1] Pallab Pradhan,[*2] Zijian Zhang,[3] Katie M. Kuo,[4] Kelsey P. Kubelick,[1,5] Da Huo,[1] Jianguo Wen,[9] Jinhwan Kim,[1,5] Zhiheng Lyu,[4] Simran Dhal,[1] Alexandra Atalis,[1] Shohini K. Ghosh-Choudhary,[10] Emily J. Devereaux,[11,12] James C.Gumbart,[3,4] Younan Xia,[1,4] Stanislav Y. Emelianov,[1,5] Nick J. Willett,[1,11,12] Krishnendu Roy[1,2,6,7,8]

[1]Wallace H. Coulter Department of Biomedical Engineering, [2]Marcus Center for Therapeutic Cell Characterization and Manufacturing; [3]School of Physics; [4]School of Chemistry and Biochemistry; [5]School of Electrical and Computer Engineering; [6]Center for ImmunoEngineering; [7]NSF Engineering Research Center for Cell Manufacturing Technologies (CMaT); [8]The Parker H. Petit Institute for Bioengineering and Biosciences, Georgia Institute of Technology, Atlanta, Georgia, USA;
[9]Center for Nanoscale Materials, Argonne National Laboratory, Lemont, Illinois, USA;
[10]School of Medicine, University of Pittsburgh, Pittsburgh, Pennsylvania, USA;
[11]Orthopaedics Department, Emory University, Atlanta, GA;
[12]Research Service, Atlanta VA Medical Center, Decatur, GA

* *These authors contributed equally to this manuscript.*

Supplementary Methods

Materials

For synthetic nanoparticle fabrication and characterization: Aminomethyl ChemMatrix resin (35-100 mesh size, ~1mmol/g loading capacity, Cat.#.68571), tris(2-carboxyethyl)phosphine (TCEP, Cat.#.646547 and C4706), and biotin (Cat.#.B4501-1G) were purchased from Sigma Aldrich. The heterofunctional crosslinker, sulfo-NHS-S-S-biotin, was purchased from ThermoFisher Scientific (Cat.#.21331), and Apexbio Technology Inc. (Cat.#.A8005). HABA (4´-hydroxyazobenzene-2-carboxylic acid) (Cat.#.28010) and avidin (Cat.#.21121) were purchased from ThermoFisher Scientific. The 30nm streptavidin-functionalized gold (Au) nanoparticles were purchased from Nanopartz Inc. (Cat.#. C11-30-TS-50) and Nanohybrids Inc. The 1.8nm, maleimide functionalized, gold nanoprobes (maleimide-Au) were also purchased from Nanopartz (Cat.#. C11-1.8-TMAL-DRY-2.5). The biotinylated quantum dots, Qdot™ 655 Biotin conjugate Kit, was purchased from ThermoFisher Scientific (Cat. #. Q10321MP). The 10 mL reaction vessel (Cat.#.SF-1000) was purchased from Torviq Inc. Human IgG1-Fc functionalized with biotin (Cat.#.IG1-H82E2) was purchased from Acrobiosystems. Peptide ligands were synthesized by Genemed Synthesis Inc. N-ethylmaleimide (NEM, Cat.#.23030), Alexa Fluor 647 C2-Maleimide (Cat.#.A20347), Alexa Fluor 680 NHS ester (Cat.#.A20008), gamma-irradiated slide-A-lyser dialysis cassettes (molecular-weight-cut-off: 2KDa, 3KDa, 10KDa) and Fisherbrand regenerated cellulose dialysis tubing (MWCO 6000-8000, Cat.#.21-152) were purchased from ThermoFisher Scientific. The 3nm biotin-Au nanoprobes (Cat.#.GNB3) were purchased from Nanocs Inc. PBS buffer was purchased from Hyclone GE Healthcare, Corning Corporation and Sigma Aldrich or made in house from monobasic (Cat.#.S9638-250G) and dibasic sodium phosphate (Cat.#.S9763-1KG) from Sigma Aldrich. Whatman Puradisc polyethersulfone syringe filter

(0.22 μm, Cat.#.6780-2502, 6780-1302) was purchased from GE Healthcare. Ultracentrifugal filters units (Amicon Ultra-4 MWCO 100 KDa) were purchased from Millipore Sigma. BD 10 mL syringes with luer lock were purchased from VWR (Cat.#.BD309653). Cyanine5-maleimide (sulfo-maleimide Cy5) and biotin Cy5 were purchased from Lumiprobe (Cat. #. 13380) and AAT Bioquest (Cat. #. 3100), respectively. Potassium cyanide (Cat.#.11813) was purchased from Sigma Aldrich. For TEM imaging, the 200-mesh formvar carbon-coated copper grids and 400-mesh ultrathin carbon film on Lacey Carbon support film copper grids were purchased from TED PELLA, Inc.

For in vitro and in vivo experiments: Ebioscience RBC lysis buffer (Cat.#. 00-4333-57), RPMI 1640 medium (Cat.#.22400105), DMEM medium (Cat. #.11995-073), OptiMEM (Cat.#.31985070) and bovine serum albumin (BSA, Cat.#.23209) were purchased from ThermoFisher Scientific. Collagenase D was purchased from Sigma-Aldrich (Cat.#.11088882001). Characterized fetal bovine serum (FBS, Cat.#.SH3007103), USDA FBS (Cat.#.SH30910.03) and 1% Penicillin-Streptomycin (PS, Cat.#.SV30010) were purchased from GE Healthcare. The recombinant murine interferon gamma (rmIFNγ) (Cat.#. 31505) protein was purchased from PeproTech. Inc. Fixation buffer (Cat.#.554655) and Alexa Fluor 647-anti-S100A9 antibodies (Cat.#.565833) were purchased from BD Bioscience. Cell strainer (Cat.#.229481) was purchased from CellTreat Inc. MACS LS columns (Cat.#.130-042-401), anti-biotin beads (Cat.#.130-105-637) and myeloid-derived suppressor cell isolation kit (MDSC-Kit, Cat.#.130-094-538) were purchased from Miltenyi Biotechnology. Purified anti-mouse CD16/32 (Clone 93, Cat.#.101302) for Fc receptor blocking and biotin anti-mouse Ly-6g/Ly-6C (Gr1, clone RB6-8C5, Cat.#.108403) for MDSC sorting was purchased from Biolegend. All antibodies used for cell marker staining includes anti-F4/80-FITC, anti-CD11c-PE, anti-B220-FITC, anti-CD8-FITC, anti-CD4-PE, anti-CD3-PE/Cy7, anti-CD11b-PE/Cy7, anti-Ly6G-PerCP/Cy5.5, anti-Ly6C-APC/Cy7,

anti-CD49b/APC, anti-FoxP3-APC and anti-CD25-APC/Cy7 were purchased from Biolegend (Please see Supplementary Table 6). Unconjugated streptavidin protein was purchased from Bio-Basic (Cat.#.SE497-5). FITC- and PE-conjugated streptavidin (Cat.#.405207, 405204) for detecting biotin-labeled cells, Zombie UV fixable dye (Cat.#.423107) and Annexin V (Cat.#.640920) were purchased from Biolegend. APC-conjugated streptavidin (Cat.#.PI21224), CellTracker Green (Cat.#.C7025) and CellTrace Yellow (Cat.#. C34573) were purchased from ThermoFisher Scientific. FACS buffer was prepared by adding 10 mL of FBS to 500 mL of PBS. MACS buffer was prepared as PBS buffer (pH7.2) containing 0.5% BSA and 2 mM EDTA. Aqua regia for dissolving tissue samples in the biodistribution study was prepared by mixing concentrated nitric acid:hydrochloride acid in 1:3 volume ratio; nitric acid (Cat.#.695025) was purchased from Sigma Aldrich; hydrochloride acid (Cat.#.BDH3030) was purchased from VWR International. Miniature screws for fixation plates in rat trauma model generation were purchased from JI Morris Co and the Gigli wire saw was purchased from RISystem, Davos, Switzerland. Mouse anti-rat His48-FITC and CD11b/c-PE antibodies were purchased from eBioscience, ThermoFisher Scientific.

Cell lines and animals

Murine triple-negative breast cancer cell line 4T1 (ATCC®CRL-2539™) and macrophage-like cell line RAW 264.7 (ATCC®TIB-71™) were purchased from American Type Culture Collection (Manassas, VA, USA). The 4T1 cell lines were cultured in RPMI 1640 medium, while RAW 264.7 cell line was cultured in DMEM medium, both supplemented with 10% FBS and 1% Penicillin-Streptomycin under standard cell culture condition (37°C, 5% CO_2).

Five to six-week-old Balb/c female mice were purchased from the Jackson Lab. Female Sprague-Dawley rats were purchased from Charles River Labs. All mice and rats

were maintained in a pathogen-free mouse or rat facility according to institutional guidelines. All of the animal experiments were approved by the Institutional Animal Care and Use Committee (IACUC) at Georgia Institute of Technology (Atlanta, Georgia, USA) and Emory University. The experimental sample sizes ensured adequate statistical power.

Supplementary Table 1: Peptide sequences and functions

Name	Sequence	Functionality
G3-biotin	WGWSLSHGYQVKK-biotin	MDSC Targeting
G3-SMCC[&]	WGWSLSHGYQVKK-SMCC	MDSC Targeting
G3*-biotin	KSLWVQWSGGHYK-Biotin	MDSC Targeting
Cp33-biotin	AQVNSCLLLPNLLGCGDDK-biotin, C6-C15 disulfide bond	FcγR Binding
Cp33-SMCC[&]	AQVNSCLLLPNLLGCGDDK-SMCC, C6-C15 disulfide bond	FcγR Binding
IrrelPep-biotin (scAHNP-biotin)	Biotin-AMFCYGVYDYCD-Amide, C4-C11 disulfide bond	Irrelevant peptide for G3, Non-targeting Peptide

&SMCC: succinimidyl 4-(N-maleimidomethyl)cyclohexane-1-carboxylate

All the peptides were synthesized by Genemed Synthesis Inc.

Preparation of MDSC-targeting SNAbs

The process to generate MDSC-SNAbs is divided into two parts: production of Janus streptavidin-coated Au nanoparticles (SA-AuNP-SHs) and surface modification of the Janus Au nanoparticles with MDSC-targeting ligands (G3 or G3*) and Fc-mimicking ligands (cp33). To generate Janus Au nanoparticles, aminomethyl ChemMatrix resins

were functionalized with biotin groups by reacting with bifunctional, thiolytic cleavable crosslinkers, sulfo-NHS-S-S-biotin in a 10 mL reaction vessel for 24 hours at 37°C with gentle rotation (step 1). As a quality control step to verify the success of the functionalization, absorbance at 260 nm of the solution in liquid phase inside the reaction vessel, which reflects the reactivity of sulfo-NHS group, was measured and compared to that of the unreacted crosslinker solution. For quantitative analysis of functionalization efficiency, HABA (4'-hydroxyazobenzene-2-carboxylic acid)/avidin assay was used to quantify the unreacted crosslinker in the liquid phase of the reaction mixture following the manufacturer's protocol. Subsequently, streptavidin-coated Au nanoparticles (SA-AuNP-SA) (Cat.# C11-30-TS-50 from Nanopartz Inc. and customized 30 nm, 100 SA/NP, streptavidin-coated Au nanospheres from Nanohybrid Inc., USA), 30 nm in diameter, were added to the reaction vessels and bound onto the resin beads by reacting with the biotins for overnight at 37°C with gentle rotation (step 2). Then, the addition of tris(2-carboxyethyl)phosphine (TCEP) released the bound Au nanoparticles into the liquid phase again by reduction of the disulfide bonds in the crosslinkers after 24 hours' reaction at room temperature (step 3). To determine the binding and cleavage efficiency, we compared the amount of Au nanoparticles collected after step 2 and 3 to the amount of SA-AuNP-SA put into the reaction vessels by measuring absorbance of solutions around the surface plasmon resonance (SPR) peak (522 nm-525 nm) of the 30 nm Au nanoparticles. To concentrate the collected Janus nanoparticles, solutions were centrifuged at 4500 g for 1 hour and the supernatant was discarded. To remove remaining TCEP, the concentrated Janus nanoparticles solution were dialyzed against PBS in gamma-irradiated, MWCO 10KDa slide-A-lyzer (ThermoFisher Scientific, USA) or washed with PBS in ultracentrifugal filter units (MWCO 100KDa, Amicon-Ultra-4) by centrifugation at 700 g for 5 min for at least four times and then stored in 4°C until use.

To modify the Janus nanoparticles, 300-fold (to the molar concentration of streptavidin) excess of the SMCC-terminated version of the desired ligands (G3-SMCC, cp33-SMCC, see Supplementary Table 1) or N-ethylmaleimide (NEM) were conjugated onto the thiol hemisphere of the nanoparticles through thiol-maleimide reaction at pH 7.4 in PBS with 0.001% Tween-20 with gentle rotating at room temperature for 4 hours or overnight at 4°C. One-fold hIgG1-Fc-biotin (InvitroGen Inc, Carlsbad, CA, USA), biotin, or 300-fold excess of biotinylated G3, G3*, cp 33, scAHNP ligands (Genemed Synthesis Inc., San Antonio, TX, USA, see Supplementary Table 1) of the molar concentration of total streptavidin molecules on the nanoparticles were coated onto the streptavidin hemisphere through streptavidin-biotin interaction in PBS with 0.001% Tween-20 with gentle rotating at room temperature for 4 hours or overnight at 4°C. Excess ligands were washed out by centrifugation at 4500 g for 50 min. Modified nanoparticles were resuspended in PBS with 0.001% Tween-20 and stored in 4°C until use. For in vitro and in vivo assays, tween-20 was removed from the nanoparticle formulation by centrifugal washes of nanoparticles with PBS.

Absorbance of NHS-leaving group

Both hydrolysis and reaction with amine groups lead to the release of sulfo-NHS as a leaving group from Sulfo-NHS-S-S-Biotin, which absorbs strongly at 260-280 nm. The absorbance of solution measured from the reaction vessels at 260-280 nm during Janus nanoparticle fabrication was used as a qualitative confirmation method to verify the functionalization of resins. A sample of the crosslinker solution before addition to the reaction vessel was measured for absorbance at 260-280 nm before and after adding NaOH (10% by volume) to determine the reactivity of the crosslinker. Another sample (100 µL) of crosslinker solution before addition to vessels was saved in 0.5 mL tube and rotated at the same time as the reaction vessels at 37 °C. The saved sample, solutions retrieved

from the vessels after reaction with the resin and the washing buffer of the last wash from the vessels were measured for absorbance at 260 nm again to validate the completion of reaction and the removal of free excess crosslinkers in the vessels after reaction. In general, the crosslinker solution retrieved from the vessels after the reaction should have higher absorbance than the saved sample of unreacted crosslinker. The washing buffer of the last wash should have the same absorbance as the PBS solution.

Quantification of the SA-AuNP-SA and SA-AuNP-SH particles

The 30 nm Au nanoparticles have a surface plasmon resonance (SPR) peak around 522 nm-525 nm. A standard curve was generated with the absorbance of a series of SA-AuNP-SA solutions of known concentrations for every new batch of SA-AuNP-SA received from Nanopartz Inc. or Nanohybrids Inc. We also measured the solutions of the SA-AuNP-SA before addition to the vessels, the solution of unbound particles after washing, and the solutions of Janus SA-AuNP-SH before and after dialysis. The calculations were done with the following equations:

$$C = k * (A_{S(522-525)} - A_{P(522-525)}) \quad \text{.....(1),}$$

Where C is the concentration of the Au nanoparticles (#/mL), k is the slope generated from the standard curve, $A_{S(522\text{-}525)}$ and $A_{P(522\text{-}525)}$ are the measured absorbance values of sample and PBS at 522-525nm respectively.

$$T = V * C \quad \text{.....(2),}$$

Where T is the total number of nanoparticles in the sample, V is the volume of the sample in milliliter.

$$P_B = 100 * (1 - \frac{T_U}{T_I}) \quad \text{.....(3),}$$

Where P_B is the percentage of nanoparticles bound onto the resins, T_U is the unbound number of nanoparticles measured out with the collected washing solution and T_I is the total input number of nanoparticles.

$$Y = 100 * \frac{T_C}{T_I} \quad \text{.....(4),}$$

Where Y is the yield of Janus SA-AuNP-SH by percentages, T_C is the total number of nanoparticles cleaved from the resins.

Verification of asymmetric surface chemistry of the Janus Au nanoparticles

To study the surface topology of the Janus nanoparticles (SA-AuNP-SH) or non-Janus nanoparticles (SA-AuNP-SA), we tagged available biotin-binding pockets or thiol groups with 10-12 nm biotinylated quantum dots (QDs) containing cadmium (Cd) or 1.8nm maleimide-Au nanoprobes and then acquired transmission electron microscopy (TEM) images with Hitachi HT7700 TEM at 120 kV (for biotinylated QD-conjugated samples) and FEI Tecnai F30 TEM at 300 kV (for 1.8 nm maleimide-Au nanoprobe-conjugated samples). The asymmetric surface chemistry of the Janus Au nanoparticles with QDs before and after modification were further investigated using advanced TEM techniques such as scanning/transmission electron microscopy (S/TEM) bright-field imaging, high-angle annular dark-field imaging (HAADF), X-ray energy dispersive spectroscopy (EDS) mapping with a ThermoFisher Scientific Talos F200X S/TEM at 200 kV. STEM-BF images are very similar to TEM images, which can reveal light elements of the streptavidin layer showing a weak dark layer surrounding Au nanoparticles. STEM-HAADF imaging has a Z-contrast (approximately proportional to Z^2) function, showing the distribution of heavy elements such as Au, Cd, Se in the imaging field, while EDS mapping helps illustrate the distribution of both the light and heavy elements in x and y directions. For sample preparation, five times excess of QDs were incubated with Janus or nonJanus Au

nanoparticles under vortex for 2 hours at room temperature. After incubation, nanoparticles were washed 3 times with DI water by centrifugation at 7500 g for 15 min. Nanoparticles were then resuspended in DI water and loaded onto the 400-mesh ultrathin carbon film on Lacey Carbon support film TEM grids for imaging. Similarly, five hundred times excess of maleimide Au nanoprobes were incubated with Janus nanoparticles and washed with DI water. The samples were then loaded onto the 200-mesh formvar carbon-coated copper grids for imaging.

Detection of thiol groups on the Janus Au nanoparticles

To verify the existence of the free thiol groups on the Janus nanoparticles, Alexa-Fluor 647-C2 maleimide dye was reacted with Janus Au nanoparticles (SA-AuNP-SH) or non-Janus Au nanoparticles (SA-AuNP-SA) for two hours at room temperature. The unreacted dye was removed by dialysis against PBS with MWCO 6000-8000 tubing for two days. The fluorescence of the dye-conjugated nanoparticle solution was read on a SynergyHT Biotek plate-reader.

Quantification of modification level using fluorophores

Twenty times excess of sulfo-maleimide Cy5 or biotin Cy5 were reacted with Janus nanoparticles (0.2 nM-0.4 nM) on vortex for 2 hours at room temperature. After reaction, nanoparticles were washed 3 times with DI water by centrifugation at 7500 g for 15 min. According to the previous report,[1] the amount of fluorophores immobilized on each Janus nanoparticle was quantified with a slight modification. Briefly, the concentration of Janus nanoparticles was first quantified by measuring the absorbance at 522-525 nm. Janus nanoparticles were then incubated at room temperature with 50 mM potassium cyanide (KCN) solution until the reddish solution became transparent to confirm the complete dissolution of gold nanoparticles. The fluorescence intensity of the sample solution was

measured with a SynergyHT Biotek plate-reader with a filter set of 590/20 (excitation), 645/40 (emission). A standard curve was obtained by measuring the fluorescence intensity of free Cy5 ranging from 0.5 to 20 nM. The average number of fluorophores per Janus gold nanoparticle was calculated by dividing the concentration of the fluorophore by the concentration of the Janus nanoparticles.

Preparation of non-Janus control nanoparticles

A stock solution of streptavidin-coated 30 nm Au nanoparticles (SA-AuNP-SA) was filtered and diluted into 1-2×10^{11} /mL in sterile PBS with 0.001% tween-20. Biotinylated peptides (*e.g.*, G3-biotin, cp33-biotin) were added in 300-fold excess to the molar concentration of total streptavidin molecules in the solution. To make double peptide-modified non-Janus nanoparticles, the G3-biotin and cp33-biotin was added in 1:1 molar ratio. The solution of nanoparticles and peptides were reacted on a rotator at 4°C for overnight. The unbound peptides were then removed by centrifugation at 5000 g for 50 min and resuspended in sterile PBS with 0.001% tween-20. The prepared peptide-modified non-Janus nanoparticles were stored in 4°C until use and washed with PBS twice by centrifugation at 5000 g for 50 min before adding to cell cultures.

Confirmation of ligand modification on Janus Au nanoparticles

The amount of ligands modified onto the surfaces of the Janus or non-Janus Au nanoparticles was determined using fluorophore-tagged ligands. Specifically, 10-molar excess of NHS-Alexa Fluor 680 (AF680) dyes were reacted onto the N-terminus of G3-biotin or cp33-SMCC ligands. Unreacted dye molecules were removed by dialysis in MWCO 2000 slide-A-lyzer cassettes. The AF680-tagged G3-biotin and cp33-SMCC were then reacted with Janus nanoparticles or non-Janus nanoparticles. The unbound peptides were again removed by dialysis against PBS in MWCO 6000-8000 dialysis tubing for two

days. Fluorescence of the nanoparticle suspension was read by a SynergyHT Biotek plate-reader at ex/em 635/680nm.

Characterization of ligand-modified nanoparticles

Sizes and zeta potentials of the ligand-modified Janus or non-Janus nanoparticles were measured in PBS (pH=7.4) using a Zetasizer Nano (Malvern, USA).

Free peptide binding on splenocytes

Two million cells of the single splenocyte suspension prepared from the 4T1-tumor-bearing mice were added to each FACS tubes. The cells were washed with PBS 1mL/tube by centrifugation at 500 g for 5 min and then resuspended into 1 mL of 0.001% streptavidin-PBS solution and incubated at room temperature for 30 min to quench the endogeneous biotin in the cells. The cells were then washed again with PBS 1 mL/tube by centrifugation and incubated with 1 mL of 0.001% biotin-PBS solution to quench the streptavidin for 30 min at room temperature. After another wash, the cells were incubated with different biotinylated peptide solutions (100 μM) in 100 μL PBS for 30 min at room temperature with at least 3 technical replicates for each type of peptides. Following the incubation with different peptide solutions and removal of excess peptides, the cells were then stained with antibodies for cell surface markers as well as the fluorescent streptavidin (streptavidin-PE or streptavidin-APC, 40 nM) for 30 min at room temperature. After washing with FACS buffer, the samples were analyzed on a BD LSRFortessa flow cytometer.

Molecular dynamics (MD) simulation of G3 and G3* peptide interaction with human S100A8/A9 heterodimer

One S100A8/A9 protein (PDB ID code 1XK4[2]) was placed in a TIP3P water box[3] of dimensions 120 x 120 x 140 Å.[4] Sixteen copies of the biotinylated G3 peptide were distributed in the unit cell such that they were at least 10 Å from S100A8/A9. NaCl ions were added to neutralize the system at a concentration of 150 mM, giving a final system size of ~200,000 atoms. Five independent systems were constructed, each with a different arrangement and orientation of the G3 peptides. Five copies of these systems were also constructed with the G3* peptides. All systems were constructed using Visual Molecular Dynamics (VMD).[4]

The CHARMM36m force field was used for proteins in all simulations[5]; biotin parameters were obtained from CGenFF[6] and used previously.[7] Temperature (310 K = 37 °C) and pressure (1 atm) were kept constant by using Langevin dynamics (damping constant γ = 1.0 ps^{-1}) and an isotropic Langevin piston barostat, respectively.[8] The time step was set to 2 fs. Bonded interactions and short-range (12-Å cutoff) nonbonded interactions were calculated at every time step. Long-range interactions were treated with the particle-mesh Ewald (PME) method[9] and were updated every other time step. A total of 10 equilibrium simulations, five for G3 and five for G3*, were run with NAMD[10] for 100 ns each.

We selected 1000 frames at equal intervals from each equilibrium simulation. Thus, a total of 5000 (1000×5) frames were used to calculate the contact probability for each type of peptide (G3 or G3*). A contact was defined as a distance of 3.5 Å or less between heavy atoms. Finally, the number of contacts was divided by 80000 (16 peptides ×1000 frames ×5 simulations) to obtain the contact probability.

Of the five systems simulated, we selected the one in which the G3 peptides have the lowest RMSD (root-mean-square-deviation) and, thus, are most stably bound to S100A8/A9. In this system, we kept the four peptides that have the lowest RMSD and reduced the size of water box to 100 x 100 x 100 Å.[4] The same approach was applied

to the G3* systems. Each of these two new systems (G3 and G3*) was run for 3.4 μs using Amber on GPUs[11]. A 4-fs time step was used with hydrogen mass repartitioning[12,13] and the pressure was maintained using the Monte Carlo barostat in Amber. The long simulation results were used to analyze the stable binding patterns between the peptides and S100A8/A9 proteins in details.

Photoacoustic Imaging of peptide-modified particles binding on cells

The isolated MDSCs or macrophages from mouse or rat were conditioned to 4 °C to prevent endocytosis of particles. Cells were then incubated with nanoparticles at a ratio of 5×10^{10}/million cells or 2×10^{11}/million cells (equal ratio in the same experiment for all particle groups) in 1mL of PBS for 1 h at 4 °C. After incubation, cells were washed three times with PBS by centrifugation at 500 g for 5 min and then fixed with BD fixation buffer. The cell-NP samples were resuspended into 20 μL per 0.5 million cells in PBS and kept at 4 °C until use.

The tissue-mimicking gelatin phantom was prepared for US/PA imaging. The phantom base layer was composed of 8% gelatin and 0.2% silica. The solution was heated to around 50 °C under stirring to dissolve the gelatin. Next, the solution was degassed to remove bubbles, poured into a container and solidified at 4 °C to form the base layer. Each cell-NP sample was mixed with an equal volume of 16% gelatin solution (heated and degassed) to prepare the cell inclusions. Once the base layer was solidified, the cell solution was pipetted onto the surface to form the cell-containing dome-shaped inclusions. The phantom was refrigerated again at 4 °C fridge to set the dome inclusions. After roughly 30 min, the phantom container was filled with ultrapure water.

The inclusions were imaged using the Vevo LAZR (Fujifilm VisualSonics Inc, Toronto, Canada) combined ultrasound and photoacoustic (US/PA) imaging system. US/PA images were acquired at a frame rate of 5 Hz with an OPO, Q-switched Nd:YAG

pumped laser (λ = 532 nm or 680 - 970 nm) with a 20 MHz US/PA linear array transducer (LZ250). Three cross-sections of each sample were randomly acquired. The data was exported and post-processed in MATLAB (Natick, MA).[14] The average PA signal was calculated for the single wavelength datasets acquired at 532 nm wavelength. PA signals from the inclusions were normalized to the PA background signal, i.e., a region containing no cells, to adjust for uncontrollable system differences between imaging frames. PA signals from the inclusions were also normalized to the corresponding average ultrasound signal. Ultrasound normalization was used to adjust for small variations in cell concentration. However, note that normalization had little impact on the imaging results, indicating similar imaging conditions and inclusion preparation were maintained, as expected.

Tumor model generation

To generate primary tumors, single cell suspension of 4T1 cells before passage 25 was prepared in PBS at a concentration of 1×10^7 cells/mL. Balb/c mice were inoculated with 0.5×10^6 4T1 breast cancer cells in 50 µL sterile PBS orthotopically into the fourth mammary fat pad of each mouse on day 0. For MDSC isolation, tumors were allowed to grow until around day 16 to 18 when a primary tumor greater than 5 mm was established.

Isolation of MDSC from the spleens of tumor-bearing mice

Balb/c mice were inoculated with 0.5×10^6 4T1 breast cancer cells on day 0. Spleens were harvested after 16-18 days from the tumor-bearing animals, minced into thin pieces, and dissociated in collagenase (2 mg/mL) in OptiMEM for 30-60 min at room temperature. Dissociated spleen tissue was passed through a 40 µm nylon cell strainer to obtain a single cell suspension. Red blood cells in the single cell suspension were lysed in 1X RBC lysis buffer. After removing the lysed RBCs by centrifugation, the splenocytes

were resuspended in RPMI 1640 complete medium and directly used for splenocyte killing experiments.

Cytotoxicity evaluation of SNAbs on MDSCs

MDSCs were isolated from the RBC-lysed single cell suspension by magnetic cell sorting with the mouse MDSC isolation kit, according to the manufacturer's protocol (Miltenyi Biotec). MDSCs (6000/well) were treated with equal amount (2-5×10^{11}/mL, 50 μL/well) of MDSC-SNAbs (Janus G3-AuNP-cp33), control particles (*e.g.*, IrrelPep-SNAbs, Janus control NPs, AuNPs), PBS buffers or DMEM medium for 4 or 24 hours at 37°C. Cells were then harvested and stained with Annexin V-APC and Zombie UV fixable dye for apoptosis and necrosis. Samples were analyzed on a BD LSRFortessa flow cytometer.

Mouse splenocyte killing of MDSCs triggered by MDSC-SNAbs

RBC-lysed splenocyte suspensions were seeded into 96 well plates at 1×10^{6} cells/well in 200 μL of RPMI 1640 complete medium. Equal amount (2-5×10^{11}/mL) of MDSC-SNAbs (Janus G3-AuNP-cp33 and G3*-AuNP-cp33), control particles (*e.g.*, Janus G3-AuNP-Fc, AuNP-G3/cp33, AuNP-cp33, AuNP) or buffers in 50 μL sterile PBS was added into the corresponding wells respectively. After 20 hours of incubation at 37°C, cells were harvested, washed and stained with antibodies for MDSCs (CD11b, Ly6G, Ly6C), macrophages (CD11b, F4/80), dendritic cells (CD11b, CD11c), T cells (CD3, CD4, CD8, Foxp3, CD25), B cells (CD3, B220), and NK cells (CD49b, CD3) (See Supplementary Table 6 for antibodies used in staining). The viability of cells was assessed by staining with Zombie UV fixable dye. FMO (fluorescence-minus-one) control samples were prepared with corresponding staining reagents. Samples were analyzed on a BD LSRFortessa flow cytometer.

Generation of rat infection trauma model

Unilateral 2.5mm femoral segmental defects were created in 21-week old female Sprague-Dawley rats as previously described. Briefly, an anterolateral incision was made along the length of the femur and the vastus lateralis was split with blunt dissection. A modular fixation plate was affixed to the femur using miniature screws (JI Morris Co., Southbridge, MA, USA). The 2.5mm segmental defect was then created in the diaphysis using a Gigli wire saw (RISystem, Davos, Switzerland). A collagen sponge with bacteria inoculum (*S. aureus* at 10^7 CFU) was placed in the defect (Supplementary Fig. 9a). The fascia was then sutured closed with absorbable 4-0 sutures, and the skin was closed with wound clips. Buprenorphine SR (0.03 mg/kg; 1 ml/kg) was used as an analgesic and applied via subcutaneous injection.

Rat MDSC-PBMC co-culture assay

Whole blood was collected via the rat tail vein longitudinally and myeloid-derived suppressor cells (MDSCs) were sorted via magnetic-activated cell sorting (MACS) using biotin-conjugated mouse anti-rat His48 antibody. FACS analysis confirmed that 88.7% of the cells in the post-sort MDSC enhanced fraction was $His48^+CD11b^+$ MDSCs (Supplementary Fig. 9b).

Myeloid-lineage cells, containing effector cells such as macrophages, were sorted from the blood of naïve rats using biotin-conjugated mouse anti-rat CD11b. Sorted trauma-associated MDSCs and $CD11b^+$ effector cells were then co-cultured at a 1:10 ratio and incubated for 24 hours with or without treatment of nanoparticles. Treatment groups included Janus nanoparticles functionalized with G3 and Pep33 (G3-SNAbs), non-Janus SA-AuNP-SA (AuNP), and no treatment. Following treatment, cells were stained with FITC-anti-rat His48 and PE-anti-rat CD11b antibodies and analyzed for the percentage of

MDSCs ($His48^+CD11b^+$ cells) remaining using a BD Accuri C6 flow cytometer. Data was analyzed using FlowJo based on fluorescent minus one (FMO) controls.

Biodistribution of MDSC-SNAbs in 4T1 murine tumor model by inductively-coupled plasma mass spectrometry (ICP-MS)

A single-cell-suspension of 4T1 cells before passage 25 was prepared in PBS at a concentration of 1×10^7 cells/mL. Five-to-six-week-old Balb/c mice were inoculated with 0.5×10^6 4T1 breast cancer cells orthotopically on the fourth mammary fat pad on day 0. Two hundred microliters of SNAbs (0.80×10^{11}) was injected via the tail vein into Balb/c mice with around 3 mm 4T1 breast tumors on day 9 post tumor inoculation. At t=6, 24, and 48 hours, the lung, liver, spleen, kidney, tumor, and blood of each mice were then harvested and weighed (n=3). Samples were then dissolved in aqua regia overnight at room temperature. Samples for ICP-MS analysis were prepared by boiling aqua regia-tissue solutions at 200 °C and then diluting the sample with DI water. The debris of tissue samples was removed with 0.2 μm syringe filters and the concentration of Au in each sample was measured by ICP-MS (NexlON 300Q, Perkin-Elmer).

In vivo depletion of MDSCs by MDSC-SNAbs in 4T1 murine tumor model

Mice of age 5-12 weeks were inoculated orthotopically with 4T1 breast cancer cells (0.5×10^6/50 μL in sterile PBS) on day 0. For single-injection groups, 200 μL of the G3-SNAb, IrrelPep-SNAb, Janus control NP, or unmodified streptavidin functionalized Au nanoparticle (SA-AuNP-SA from Nanohybrids Inc) formulation containing 7.5×10^{10} nanoparticles were administered intravenously through tail vein injection into the mice on day 10 post tumor inoculation. For G3-SNAb three-injection group, SNAbs were administered intravenously on day 6, 8, and 10 post tumor inoculation. On day 11, mice were euthanized. Spleens and tumors were collected and processed as described

previously. Briefly, spleens and tumors were treated with collagenase D and RBC lysis buffer to generate single cell suspensions. We also collected blood by cardiac puncture. One hundred microliters of blood from each mouse was transferred to fresh FACS tubes treated with 2 mL RBC lysis buffer at room temperature for 10 min, and centrifuged at 700 g for 10 min. The supernatant was discarded and RBC lysis was repeated once again. Cell pellets were resuspended in FACS buffer and stained with antibodies for MDSCs (CD11b, Ly6G, Ly6C), macrophages (CD11b, F4/80), dendritic cells (CD11b, CD11c), T cells (CD3, CD4, CD8, Foxp3, CD25), B cells (CD3, B220), and NK cells (CD49b, CD3). FMO (fluorescence-minus-one) control samples were prepared with corresponding staining reagents. Samples were run on a BD LSRFortessa flow cytometer.

Statistical analysis

Statistical analysis was performed using GraphPad Prism software. Shalpiro-Wilk test was used to determine the normality of data in each experiment. ROUT method with Q=1% was used to identify outliers. For in vivo depletion experiments, animals were also excluded from analysis if over half of the primary tumor established was found to be intraperitoneal on the day of dissection, indicating tumor inoculation failure. To determine statistical differences between two groups with normal Gaussian distributions, a Student's t-test (two-tailed, unpaired, unequal variance, $p<0.05$) was performed. To determine if statistical differences were significant between three or more groups, with normal Gaussian distributions, one-way ANOVA was performed followed by a post-hoc Tukey's test. To determine if statistical differences were significant between three or more groups, with non-normal distributions, Kruskal-Wallis test was performed followed by a post-hoc Dunn's multiple comparison test.

Supplementary Figures

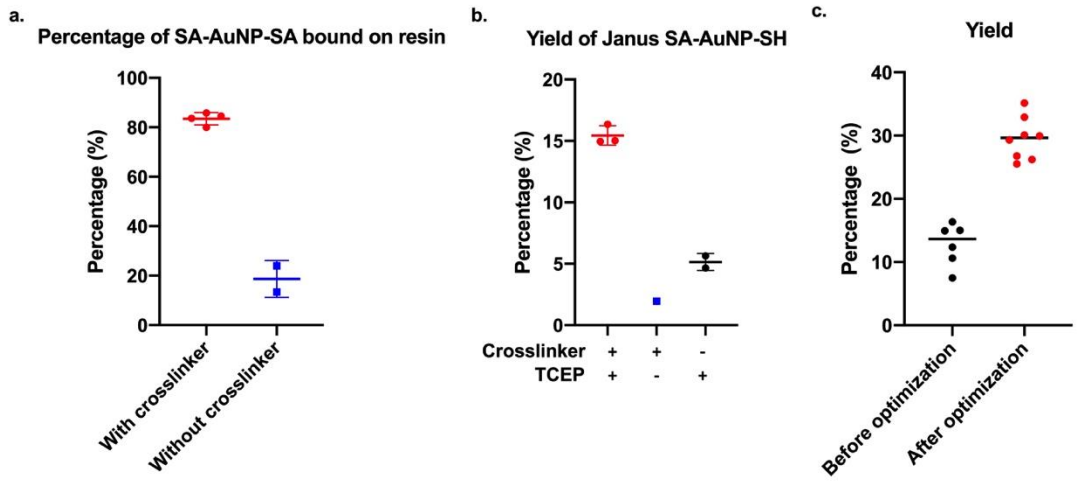

Supplementary Figure 1. Validation of the solid-phase-chemistry-based Janus nanoparticle fabrication method. (a) The percentage of SA-AuNP-SA bound on the resins with or without crosslinker functionalization. Data are presented as mean ± s.d. N=2 independent samples with n=2 or 4 technical replicates. (b) The yield of Janus SA-AuNP-SH with or without crosslinker functionalization of resin or TCEP for cleavage of nanoparticles from resin. Data are presented as mean ± s.d. N=3 independent samples with n=1, 2 or 3 technical replicates. The data are representative of at least five independent experiments. (c) Increase of yield after optimizing solid phase chemistry fabrication procedure. Yield of Janus SA-AuNP-SH increased after optimization of input material ratio and concentration and reaction conditions (pH, ionic strength of buffer, temperature, reaction duration, mixing method). When the ratio between the bound biotin on the resin and the total number of streptavidin on the input SA-AuNP-SA nanoparticles was between 1.8×10^5:1 to 3.6×10^5:1, 60%-90% of the input Au nanoparticles could be bound onto the functionalized resins and 20%-40% of the total input Au nanoparticles could be cleaved off the resins and collected as Janus nanoparticles (SA-AuNP-SH). Data are presented as mean ± s.d. In (c) data of before optimization group is from n=6 technical replicates from three independent experiments. Data of after optimization group is from n=8 technical replicates from two independent experiments.

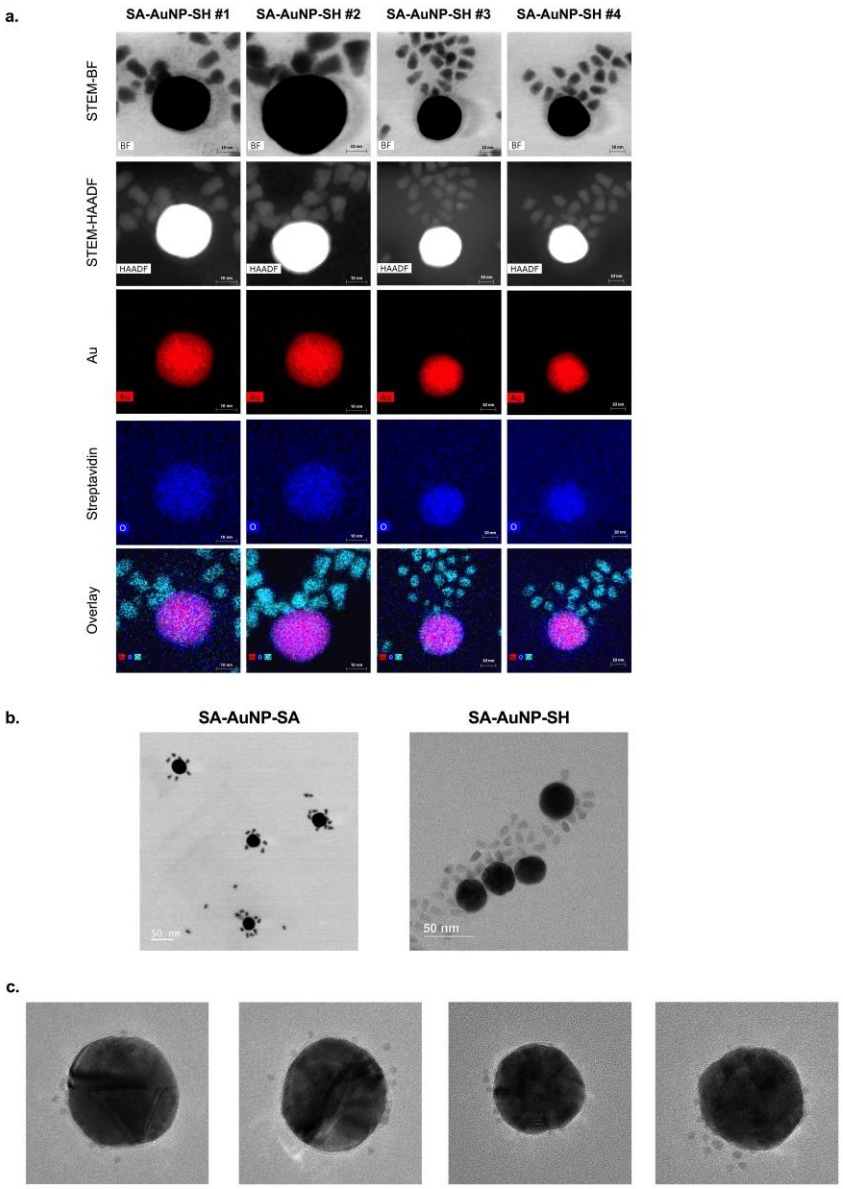

Supplementary Figure 2. Validation of asymmetric surface chemistry of the Janus nanoparticles (SA-AuNP-SHs). (a) S/TEM-BF images, STEM-HAADF images, and EDS mapping images of biotinylated quantum dot (QD)-conjugated Janus gold nanoparticles. Colors: red-gold (nanoparticles), blue-oxygen (streptavidin), cyan blue-Cadmium (biotinylated QDs). SA-AuNP-SH #2 is also used in Figure 2 in the main paper. (b) Bright field TEM/STEM image of multiple nonJanus (left, taken by ThermoFisher Scientific Talos F200X S/TEM at 200 kV) or Janus nanoparticles conjugated with biotinylated QD (right, taken by Hitachi HT7700 TEM at 120 kV). Only part of the surface of the Janus nanoparticles was coated with QDs while nonJanus nanoparticles were coated with QDs all over the surfaces. (c) TEM images of Janus nanoparticles conjugated with 1.8 nm maleimide-Au nanoprobes. Only part of the surface of the Janus nanoparticles was coated with maleimide nanoprobes.

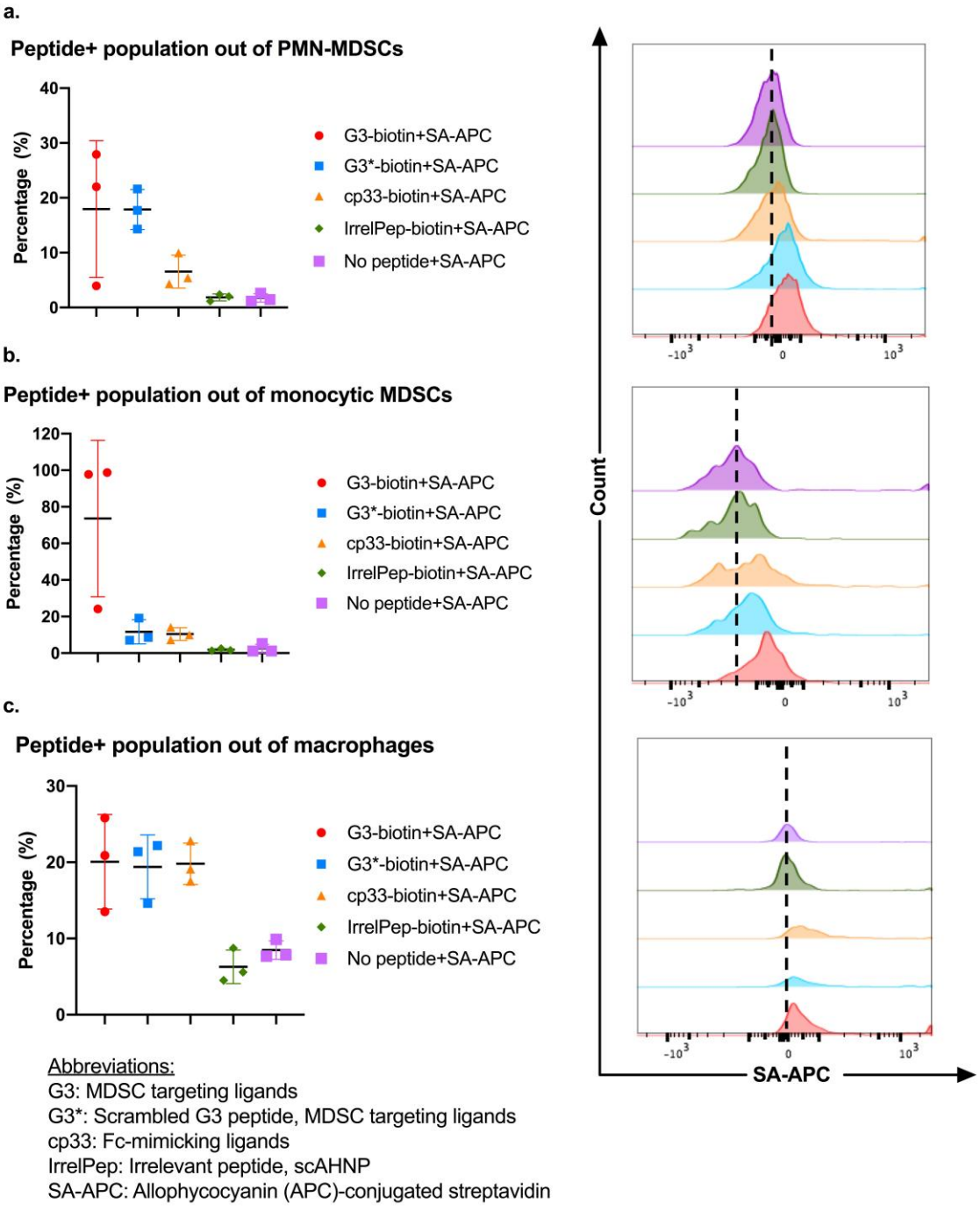

Supplementary Figure 3. Free peptide binding on MDSCs and macrophages in a mixture of splenocytes. Single-cell suspension of splenocytes containing MDSCs, macrophages, DCs, NK cells, B and T cells were quenched for endogenous biotin and then incubated with different solutions of free biotinylated peptides for half an hour followed by staining with fluorescent streptavidin and analysis by flow cytometry. Left graphs show the percentage of cells with bound peptides out of PMN-MDSCs (a), M-MDSCs (b), macrophages (c) after staining with allophycocyanin (APC)-conjugated streptavidin (SA).

The right graph shows the fluorescence intensity of the corresponding populations in the APC channel. Data are presented as mean ± s.d. with n=3 technical replicates. The dashed lines in the right graphs mark the peak of the no-peptide-control samples.

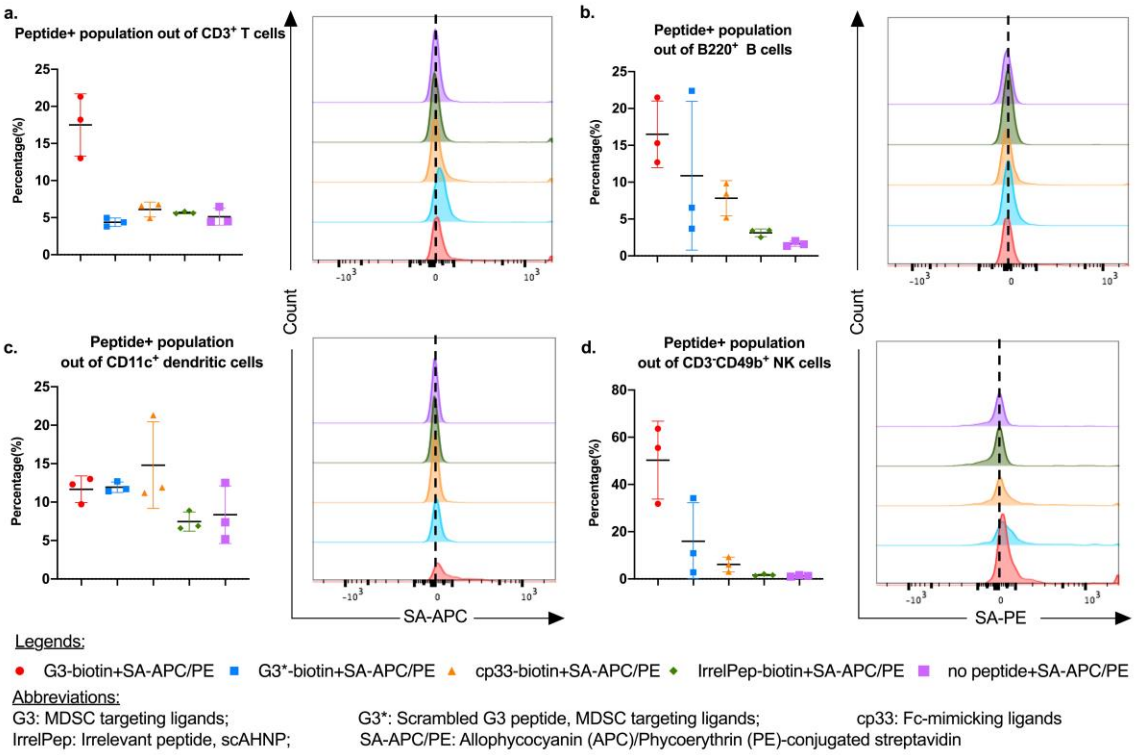

Supplementary Figure 4. Free peptide binding on T cells, B cells, DCs and NK cells in a mixture of splenocytes. Single-cell suspension of splenocytes containing MDSCs, macrophages, DCs, NK cells, B and T cells were quenched for endogenous biotin and then incubated with different solutions of free biotinylated peptides for half an hour followed by staining with fluorescent streptavidin (SA) and analysis by flow cytometry. Left graph shows the percentage of cells with bound peptides out of $CD3^+$ T cells (a), $B220^+$ B cells (b), $CD11c^+$ DCs (c), $CD3^-$ $CD49b^+$ NK cells (d) in a single-cell suspension of splenocytes after staining with SA-APC (allophycocyanin) or SA-PE (Phycoerythrin) and the right graph shows the fluorescence intensity of the corresponding populations in the APC or PE channel. Data are presented as mean ± s.d. with n=3 technical replicates. The dashed lines in the right graphs mark the peak of the no-peptide-control samples.

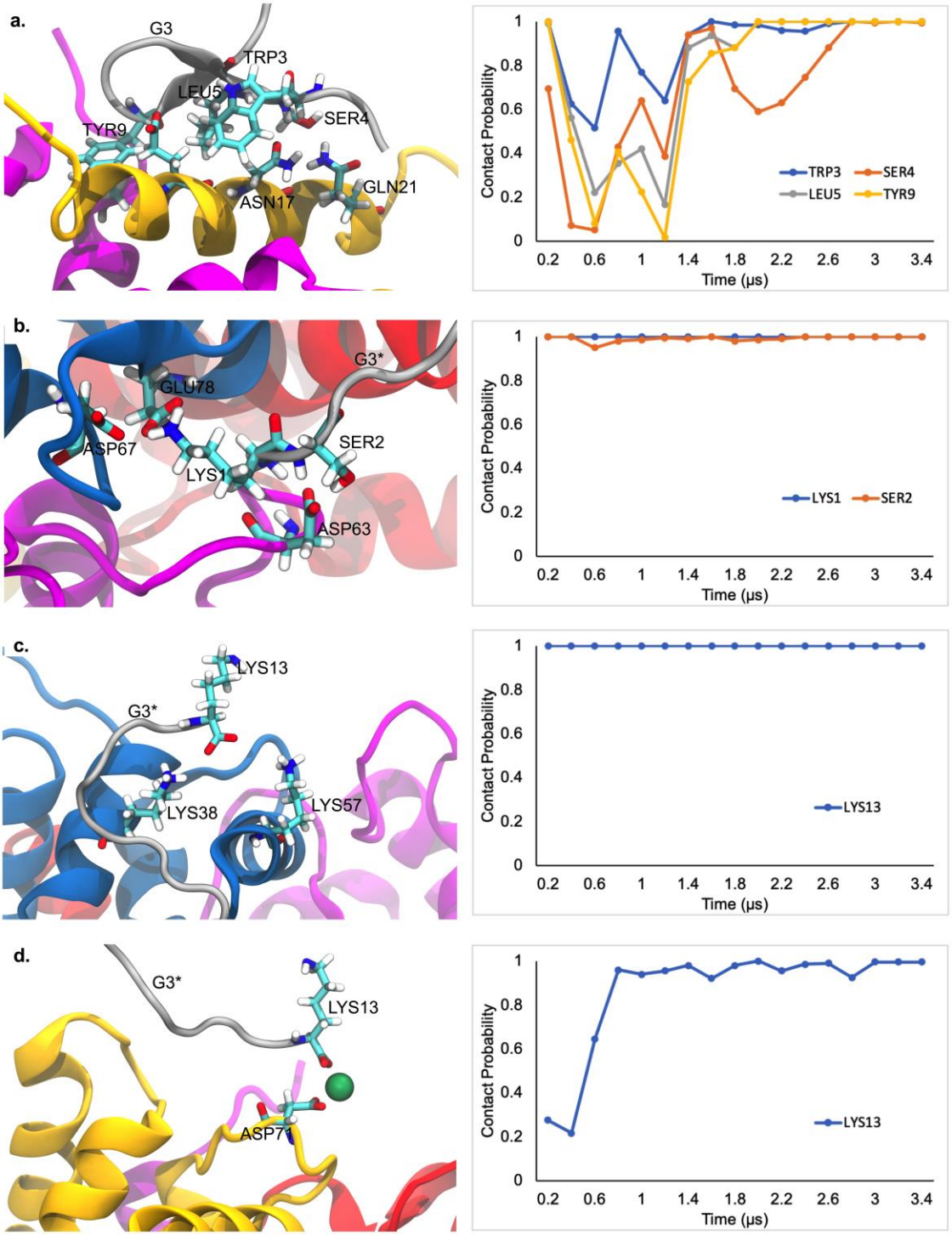

Supplementary Figure 5. Two long simulations (3.4-μs each) reveal several stable binding patterns between human heterotetramer S100A8/A9 and G3 (1 peptide) and G3* (3 peptides). (a)-(d) Stabilizing interactions between S100A8/A9 (red, blue, magenta, yellow) and peptide (grey). (a) Two hydrogen bonds and hydrophobic interactions help G3 to bind to S100A8/A9. (b) Hydrogen bonds at the N-terminal side of G3* with S100A8/A9

protein. (c) Hydrogen bonds between G3* C-terminus and S100A8/A9. (d) Calcium cation (green) electrostatically interacts with G3* backbone at C-terminus. The adjacent plot of each figure is contact probability between the residues and S100A8/A9 proteins (defined as within 3.5 Å, every 200 ns period) in the simulations.

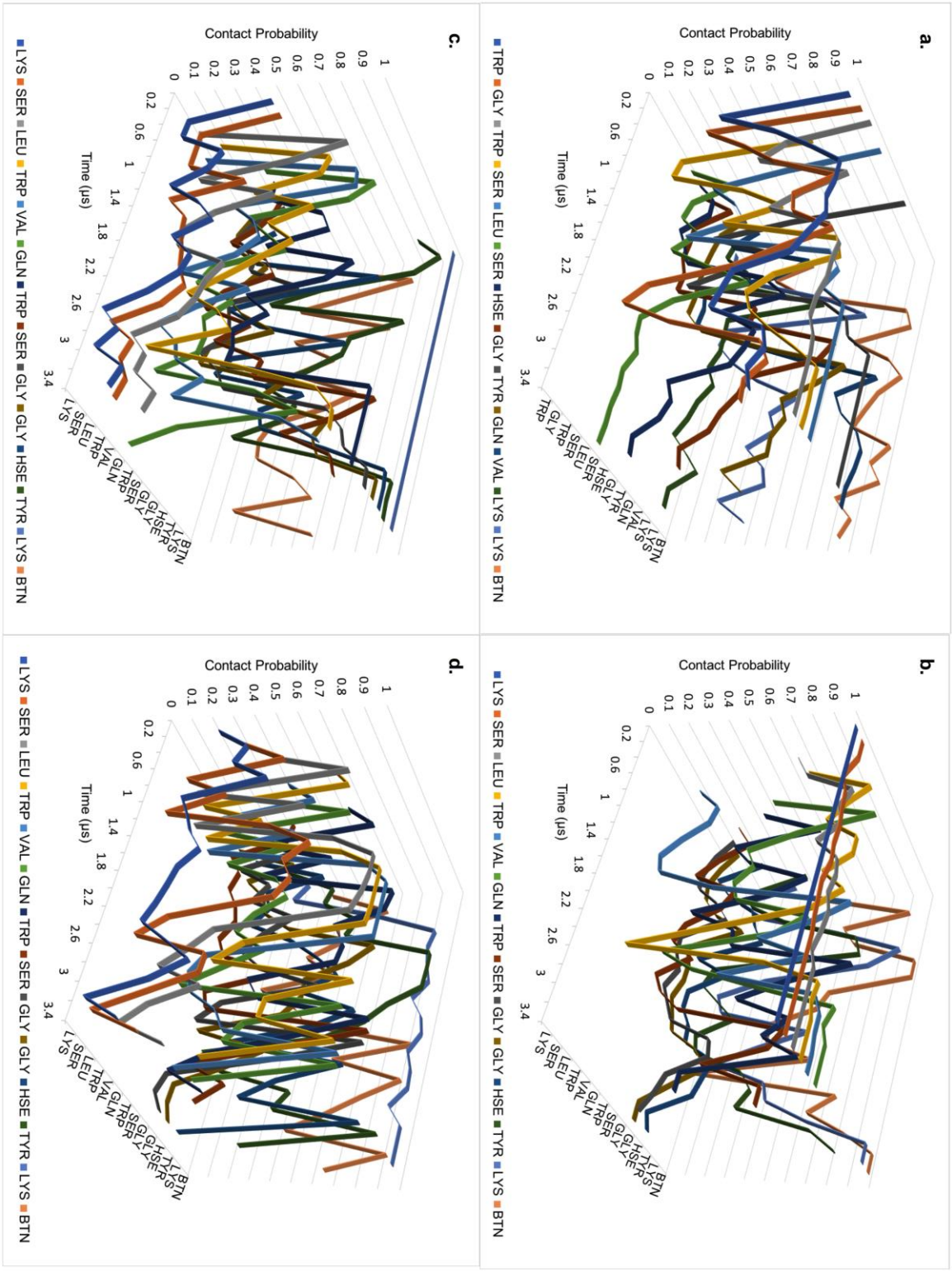

Supplementary Figure 6. Contact probability per residue for the peptides (G3, G3*) and S100A8/A9 in the long simulations (3.4-μs each). (a)-(d) The graphs show the contact probability per residual of G3 and S100A8/A9 (a) and each of three copies of G3* and

S100A8/A9 (b-d). In G3, Lys12 and Lys13 are not involved in binding to S100A8/A9, indicated by their low contact probability, and instead they form intrapeptide interactions. In G3*, the two lysines are located separately at the N- and C-termini (not counting biotin), and both play a role in binding to S100A8/A9.

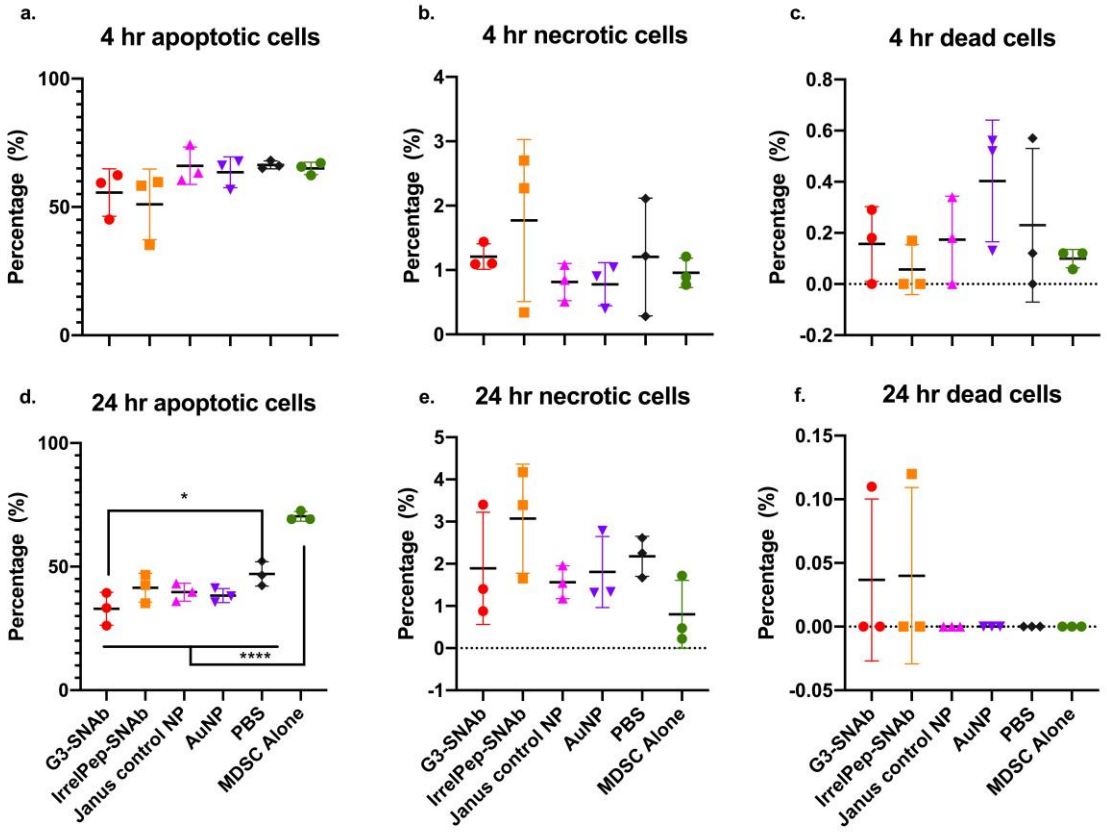

Supplementary Figure 7. Toxicity of SNAbs on MDSCs isolated from 4T1-tumor-bearing mice. MDSCs were incubated with the Janus nanoparticles, i.e., G3-SNAbs (Janus G3-AuNP-cp33), IrrelPep-SNAb (Janus scAHNP-AuNP-cp33), and Janus control NP (biotin-AuNP-NEM), or AuNP, PBS or DMEM medium for 4 hours or 24 hours. The viability of MDSCs was evaluated with Zombie UV fixable kit and Annexin V-APC at the two time points. (a-f) The graphs show the percentage of apoptotic (Zombie UV-Annexin V+), necrotic (Zombie UV+Annexin V-), and dead (Zombie UV+Annexin V+) cells at 4 hour (a-c) and 24 hour (d-f), respectively. Data are presented as mean ± s.d. with n=3 technical replicates.

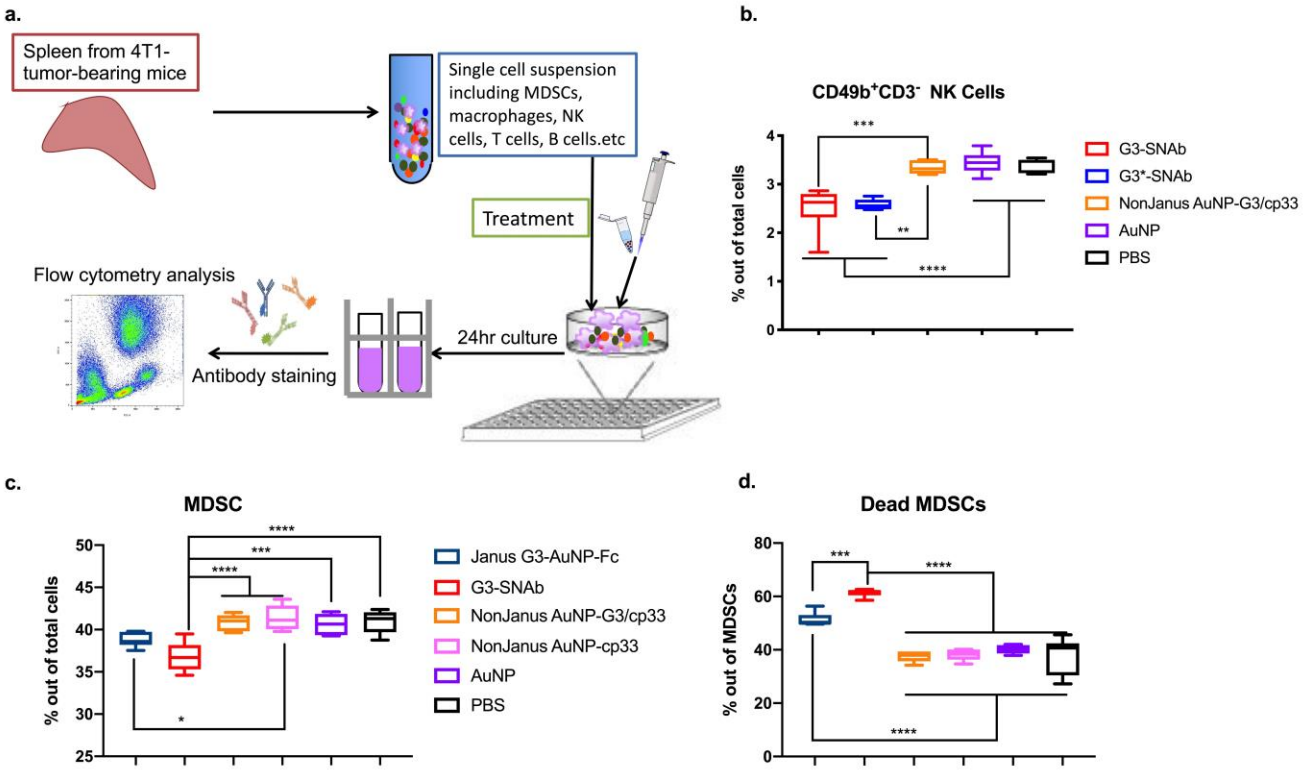

Supplementary Figure 8. MDSC-SNAbs induce antibody-like killing of mouse MDSCs in splenocyte suspension containing effector cells. (a) In the splenocyte suspension assay, the spleens were isolated from 4T1-tumor-bearing mice and treated with equal amount of different types of nanoparticles for 24 hours. After treatment, the cells were stained with fluorescent antibodies and fixable Zombie UV viability dye and analyzed for the percentage and viability of various types of cells (e.g., MDSC, F4/80$^+$ macrophages, CD11c$^+$ DCs, T cells, B cells and NK cells). (b-d) The percentage of CD3$^-$CD49b$^+$ NK cells (b), the percentage of MDSC (PMN-MDSC and monocytic MDSC) out of total cells (c) and percentage of dead cells out of MDSCs (d) in the splenocyte suspension after different treatments. Data are presented in box plots (n=6). Significance was determined using one-way ANOVA with Tukey post-hoc test (**** $p<0.0001$, *** $p<0.0002$, ** $p<0.0021$, * $p<0.0332$). AuNPs are non-Janus streptavidin coated Au nanoparticles. NonJanus AuNP-G3/cp33 nanoparticles are AuNPs coated with randomly distributed G3 and cp33. NonJanus AuNP-cp33 nanoparticles are AuNPs coated with biotinylated cp33. G3-SNAb and Janus G3-AuNP-Fc are Janus AuNP coated with both G3 and cp33 or Fc fragment in spatially segregated area. Similarly, G3*-SNAb are Janus AuNP coated with G3* and cp33.

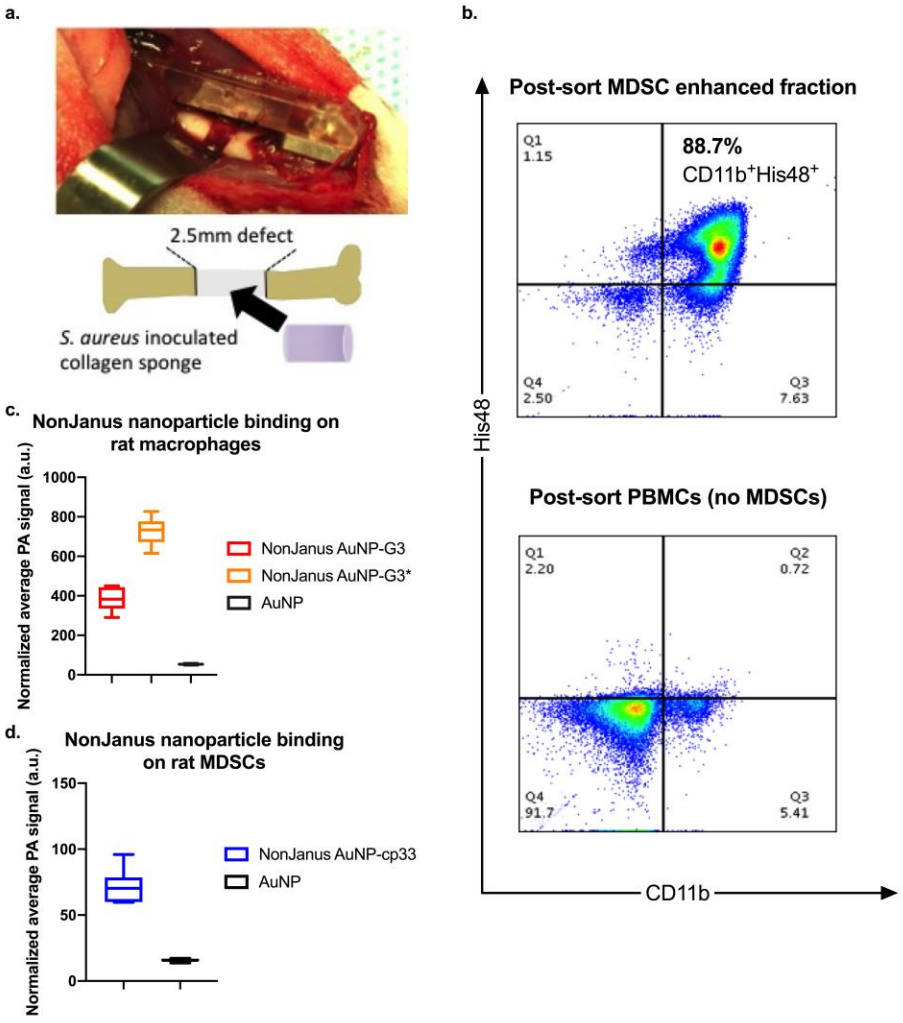

Supplementary Figure 9. Rat bone trauma model for MDSC isolation and nonJanus nanoparticle binding on rat MDSCs and macrophages. (a) Unilateral 2.5mm femoral segmental defects were created in 21-week old female Sprague-Dawley rats. A collagen sponge with bacteria inoculum (S. aureus at 10^7 CFU) was placed in the defect to induce infection. (b) MDSC were sorted via magnetic-activated cell sorting (MACS) using biotin mouse anti-rat His48 antibody from blood of the rats. The purity of $CD11b^+His48^+$ cells was 88.7% in the post-sort MDSC enhanced fraction. (c,d) Rat macrophages and MDSCs treated with the same amount of different nonJanus nanoparticles were anlalyzed using photoacoustic imaging techniques. (c,d) The relative amount of nanoparticles bound to rat macrophages (c) or MDSCs (d) based on the average PA signals of each cell inclusion (0.5 million cells/40 μL). PA signals shown in the graphs were normalized against the laser energy and backscattered ultrasound signals. Data are presented as mean ± s.d. of at least three cross-section images of corresponding independent samples.

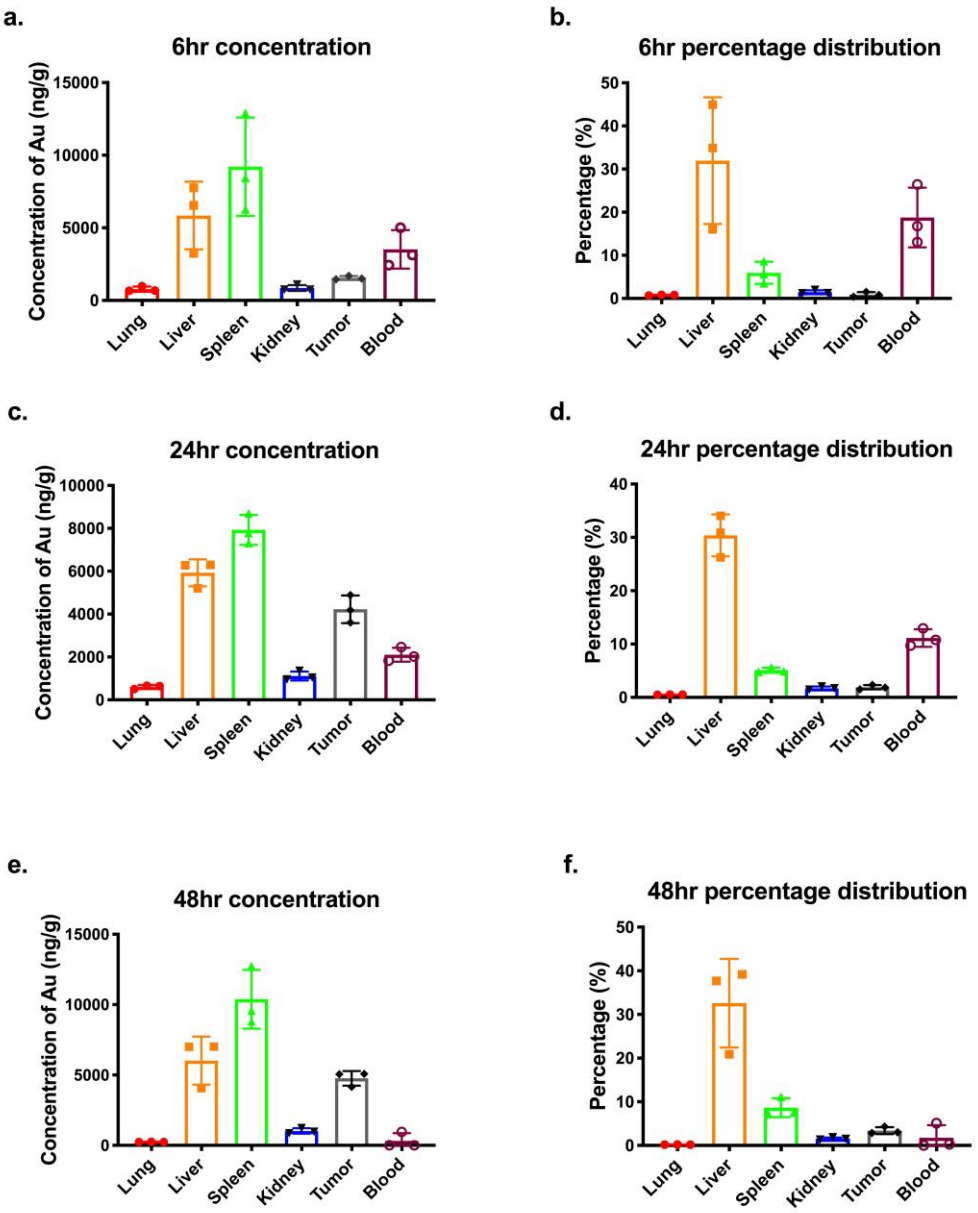

Supplementary Figure 10. Biodistribution of MDSC-SNAbs after intravenous injection in a 4T1 mouse breast cancer model. G3-SNAbs were administered through tail vein injection on day 9 post tumor inoculation. Lung, liver, spleen, kidney, tumor and blood were harvested after 6, 24, or 48 hours for ICP-MS analysis. The concentration of SNAbs (ng of Au per g of tissue) and calculated percentage of SNAbs out of the total injected amount in each organ at each time point (a-b. 6 h; c-d. 24 h; e-f. 48 h) were plotted with mean ± s.d. of 3 biological samples (n = 3).

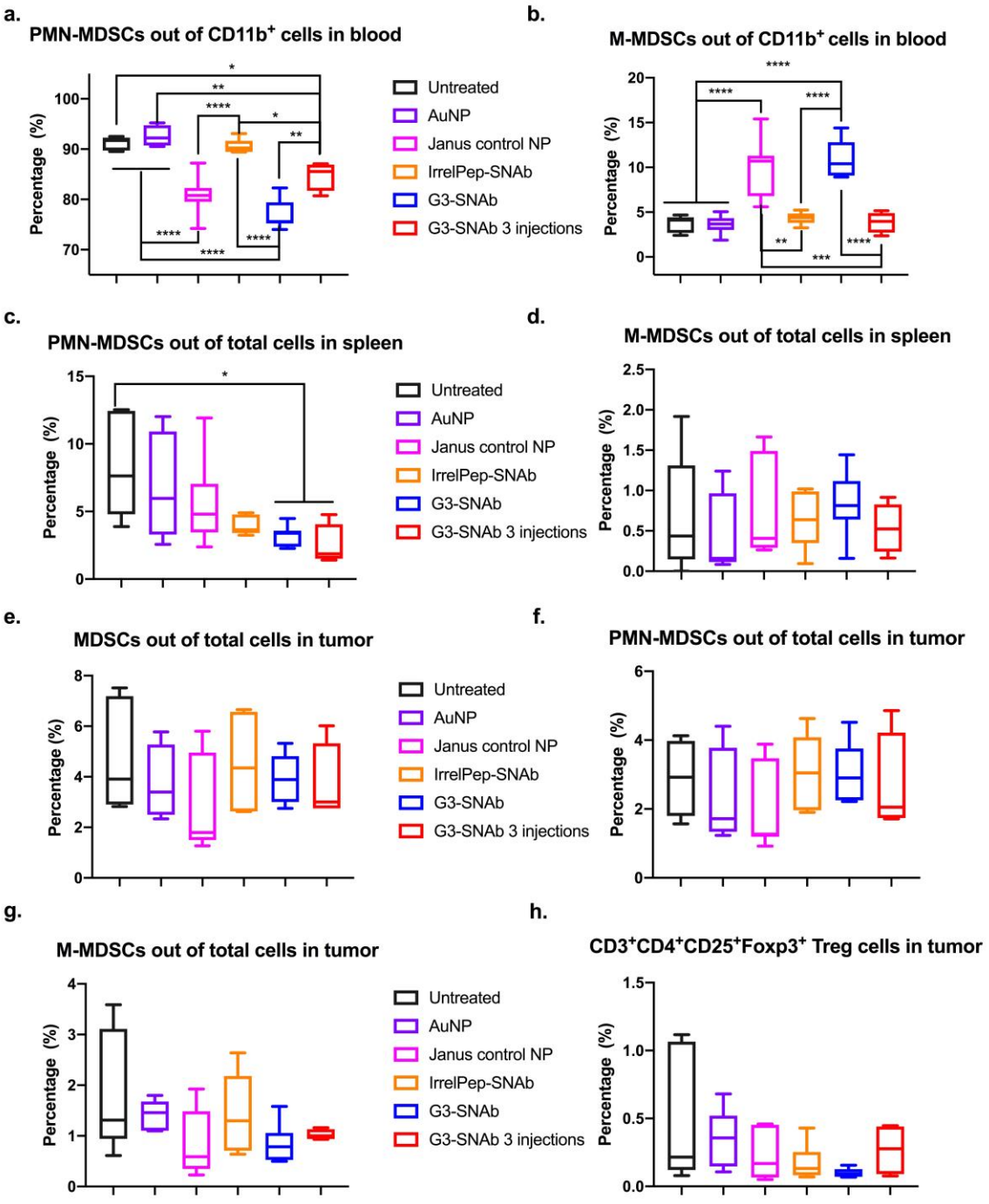

Supplementary Figure 11. Treatment effect of MDSC-SNAbs in 4T1 murine tumor model. The percentages of total MDSCs in the tumor (e), PMN-MDSCs (a, c, f) and M-MDSCs (b, d, g) in blood, spleen and tumor out of total cells in each organ, and the percentage of $CD3^+CD4^+CD25^+Foxp3^+$ Treg cells (h) in the tumor are presented in box plots with box showing median, 25 and 75 percentile and whiskers showing min and max. n=6 for untreated group, n=6 (a, b, e-h) and n=7 (c-d) for AuNP, n=7 for Janus control NP, n=5 (a-d) and n=6 (e-h) for IrrelPep-SNAb group, and n=6 (h) and n=7 (a-g) for G3-SNAb

single injection group, n=4 for G3-SNAb three injections group. Significance was determined using one-way ANOVA with Tukey post-hoc test for data (**** p<0.0001, *** p<0.0002, ** p<0.0021, * p<0.0332).

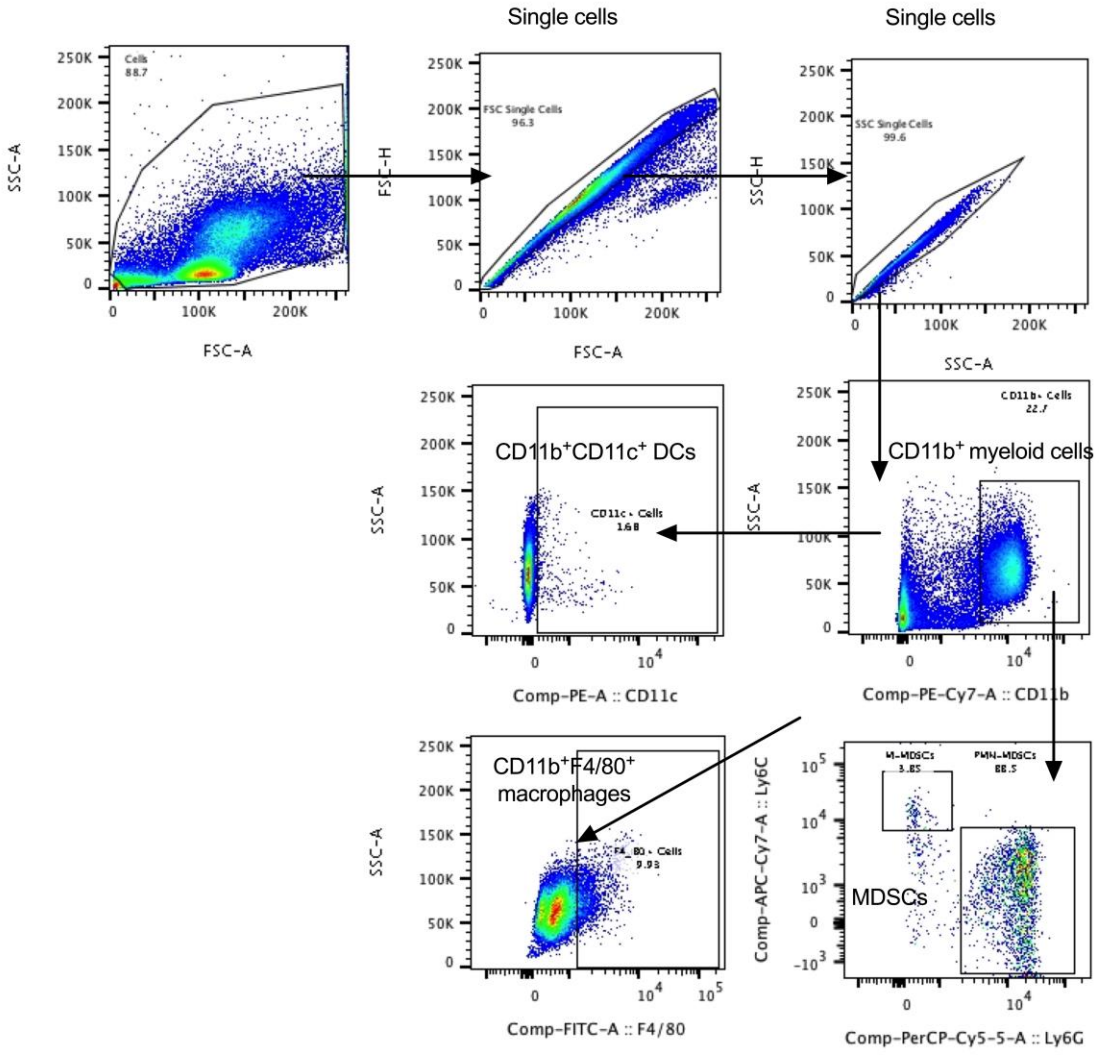

Supplementary Figure 12. Gating strategy for DCs, macrophages, PMN-MDSCs and M-MDSCs in animal studies. $CD11b^+$ cells were gated out from single cell suspension first and $CD11b^+$ $CD11c^+$ DCs, $CD11b^+F4/80^+$ macrophages, $CD11b^+Ly6G^+Ly6C^{low}$ PMN-MDSCs and $CD11b^+Ly6G^-Ly6C^{high}$ monocytic MDSCs were gated out from $CD11b^+$ cells. Gating was set by FMO (fluorescence-minus-one) controls. Representative flow plots are from spleen samples.

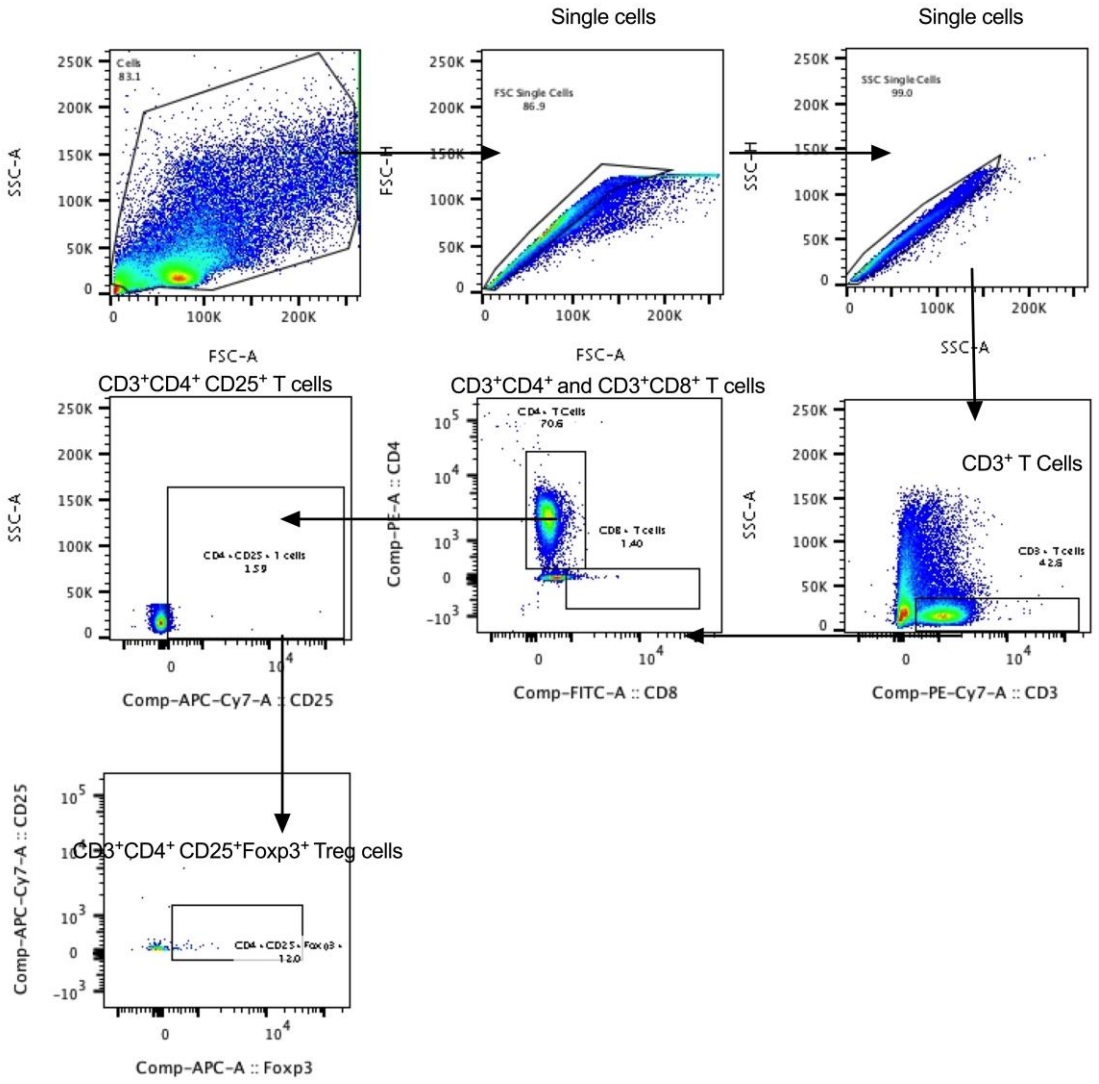

Supplementary Figure 13. Gating strategy for T cell populations in animal studies. $CD3^+$ cells were gated out from single cell suspension first and the two subsets of T cells ($CD3^+CD4^+$ helper T cells and $CD3^+CD8^+$ cytotoxic T cells) were gated out from $CD3^+$ cells. Next, $CD3^+CD4^+CD25^+$ T cells were gated out from $CD3^+CD4^+$ helper T cell subset and $CD3^+CD4^+CD25^+FoxP3^+$ regulatory T cells were gated out from the $CD3^+CD4^+CD25^+$ T cell population. Gating was set by FMO (fluorescence-minus-one) controls. Representative flow plots are from tumor samples.

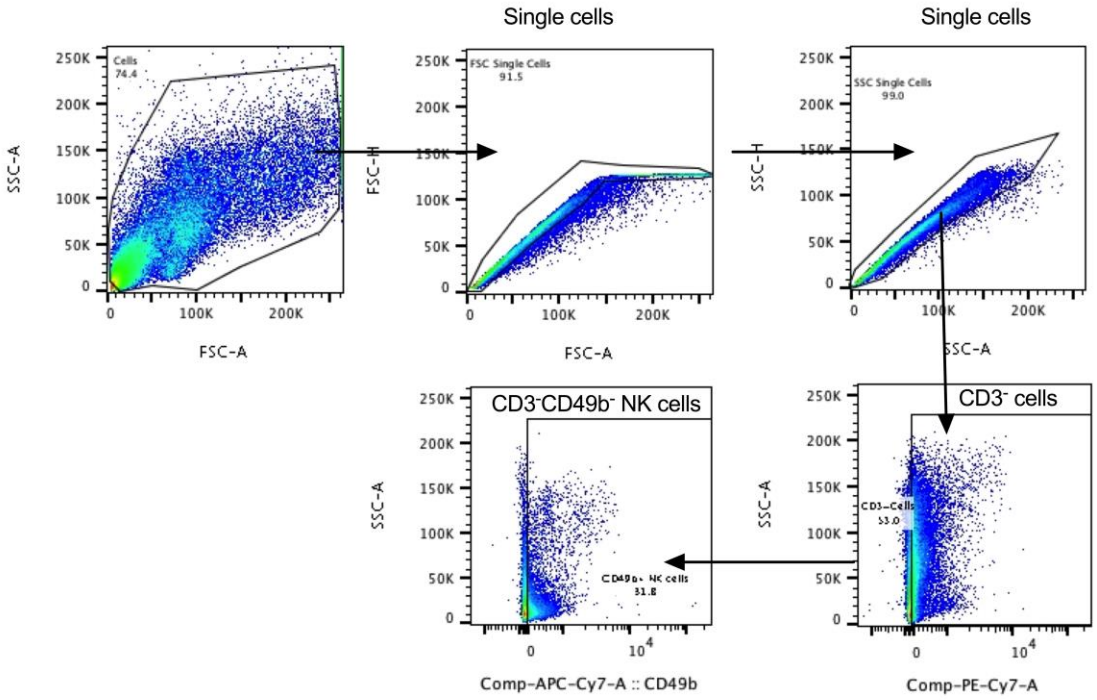

Supplementary Figure 14. Gating strategy for $CD3^{-}CD49b^{+}$ NK cell population in animal studies. $CD3^{-}$ cells were gated out from single cell suspension first and $CD3^{-}CD49b^{+}$ NK cells were gated out from $CD3^{-}$ cells. Gating was set by FMO (fluorescence-minus-one) controls. Representative flow plots are from tumor samples.

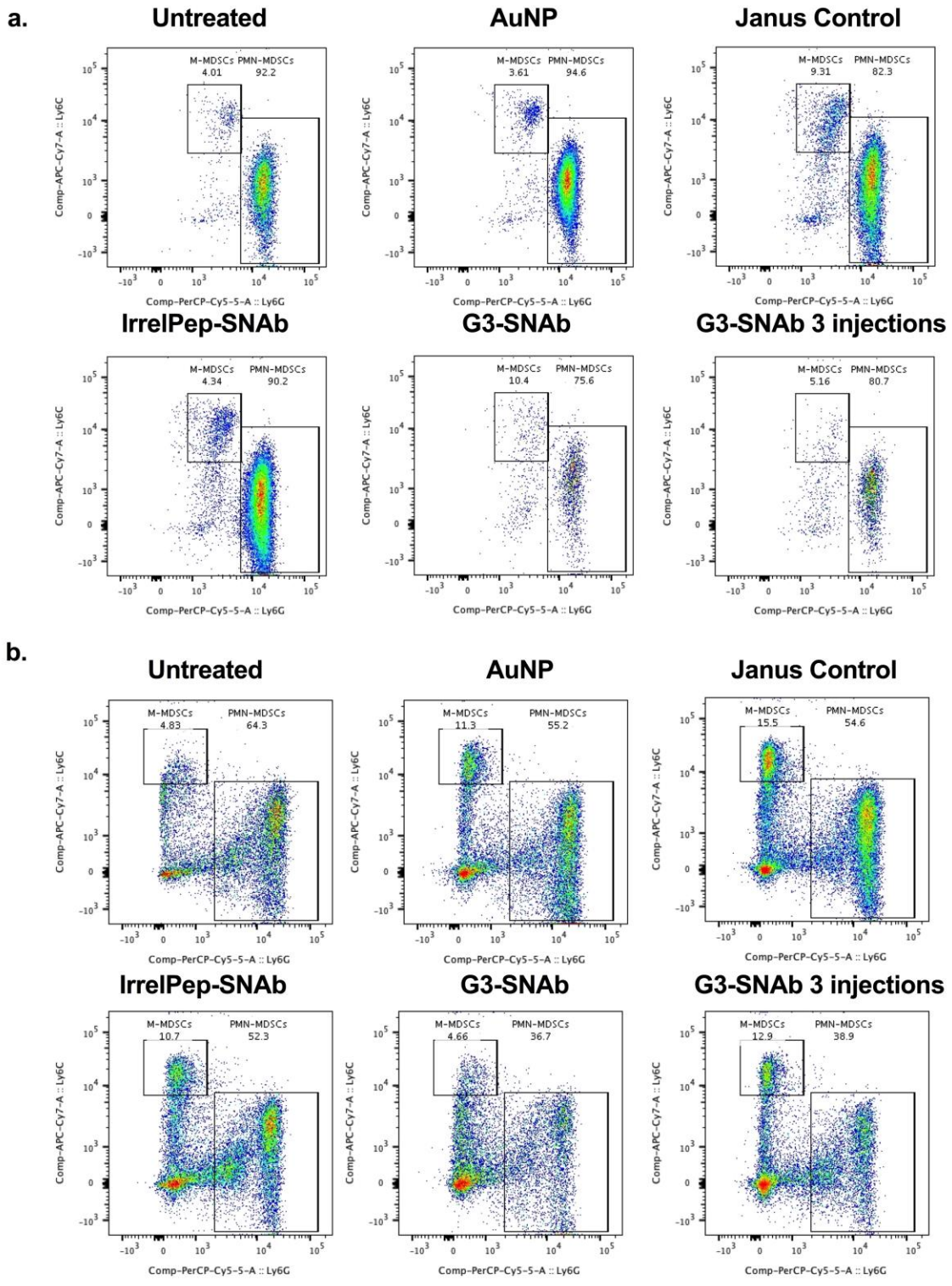

Supplementary Figure 15. Representative flow cytometry scattering plots of PMN-MDSCs and M-MDSCs out of CD11b^{+} cells in blood (a) and spleen (b) after treatment at Day 11 post tumor inoculation in the 4T1-tumor bearing mice. Gating was set by fluorescence-minus-one (FMO) controls.

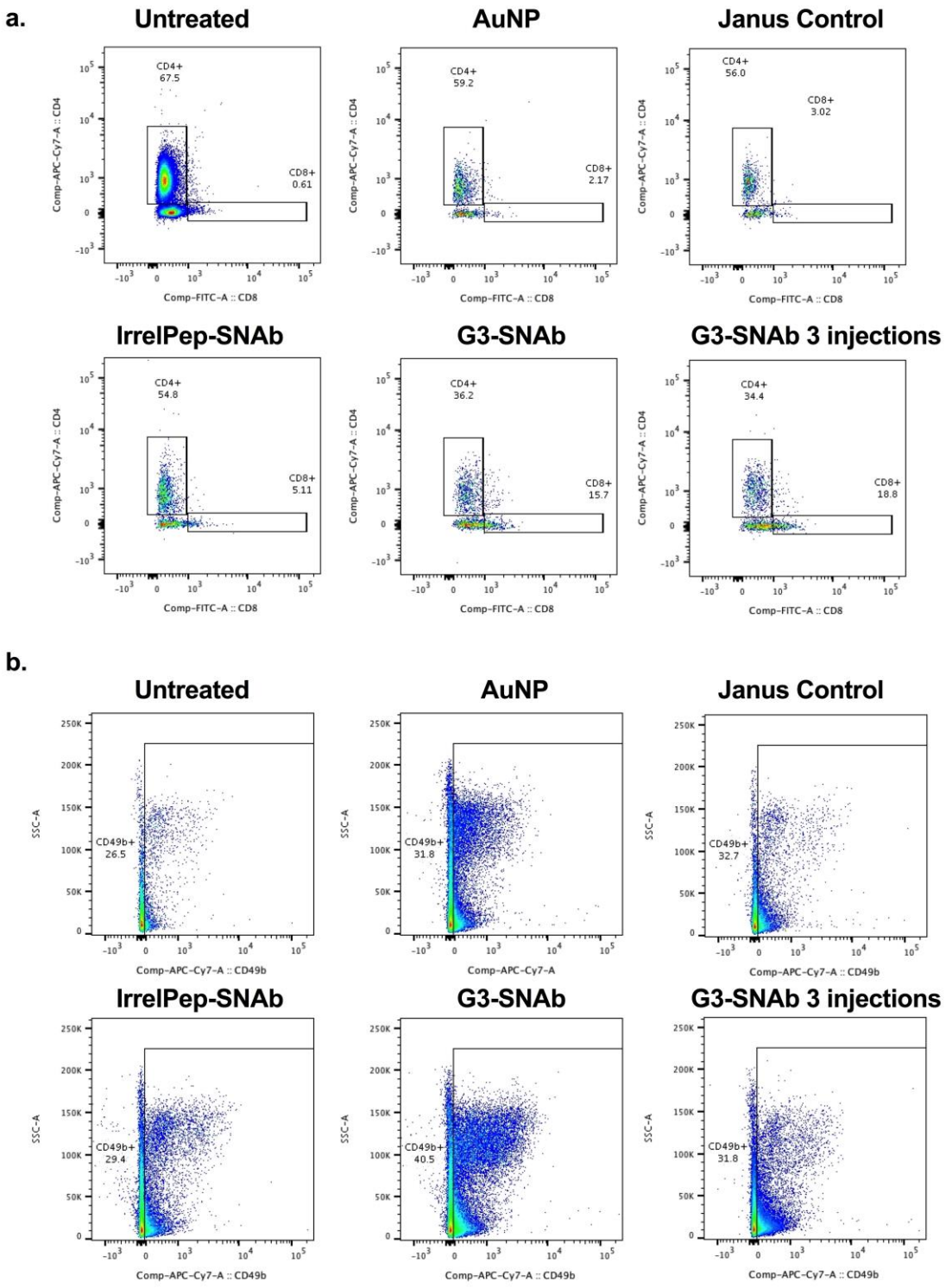

Supplementary Figure 16. Representative flow cytometry scattering plots of $CD3^{+}CD8^{+}$ T cells out of $CD3^{+}$ T cells (a) as well as $CD3^{-}CD49b^{+}$ NK cells out of $CD3^{-}$ cells (b) in tumors after treatment at Day 11 post tumor inoculation in the 4T1-tumor bearing mice. Gating was set by fluorescence-minus-one (FMO) controls.

Supplementary Table 2. Modification level of Janus nanoparticles.

Modification Level (molecule per NP)	Biotin Cy5	Sulfo-maleimide Cy5
Average	13.11	15.66
ST.DEV	2.27	2.10

Supplementary Table 3. Typical sizes of the Janus nanoparticles.

Size	Janus Nanoparticles				AuNP
	G3-AuNP-Fc	G3-SNAb	G3*-SNAb	IrrelPep-SNAb	
Ave. Size (nm)	178.9	95.04	92.14	90.80	73.79
ST.DEV (nm)	103.7	41.5	39.93	34.73	22.15

Supplementary Table 4. Typical sizes of modified non-Janus nanoparticles

Size	NonJanus Nanoparticles		AuNP
	AuNP-G3/cp33	AuNP-cp33	
Ave. Size (nm)	83.69	79.96	73.79
ST.DEV (nm)	28.87	29.58	22.15

Supplementary Table 5. Typical zeta potential of SNAbs

Particle Type	Ave. Zeta Potential (mV)	ST.DEV (mV)
AuNP	-3.50	2.17
Janus control NP	-3.68	0.87
G3-SNAbs	-3.54	0.47
IrrelPep-SNAbs	-2.31	0.64

Supplementary Table 6. Antibodies used in flow cytometry and MACS sorting.

Flow Cytometry			
Name	Clone	Company	Function
APC Annexin V	Annexin A5	Biolegend	Apoptotic cells
APC Anti-Foxp3	FJK-16s	eBioscience	Treg
APC anti-mouse CD49b (pan-NK cells)	DX5	Biolegend	NK cells
APC/Cy7 Anti-mouse CD4	RM4-5	Biolegend	T cell
APC/Cy7 Anti-CD49b (pan-NK cells)	DX5	Biolegend	NK cells
APC/Cy7 anti-mouse CD25	3C7	Biolegend	Treg
APC/Cy7 anti-mouse Ly-6C	HK1.4	Biolegend	Mouse MDSC
FITC anti-mouse CD8a	53-6.7	Biolegend	T cell

Supplementary Table 6 Continued

FITC anti-mouse/human CD45R/B220	RA3-6B2	Biolegend	B cell
FITC anti-mouse F4/80	BM8	Biolegend	Mouse Macrophages
PE anti-mouse CD4	RM4-5	Biolegend	T cell
PE anti-mouse CD11c	N418	Biolegend	DC
PE anti-mouse CD32b	AT130-2	eBioscience	FcγRIIb
PE Anti-Ki-67	SolA15	eBioscience	Proliferation
PE anti-mouse Perforin	S16009A	Biolegend	Cytolytic activity
PerCP/cy5.5 anti-human/mouse Granzyme B	QA16A02	Biolegend	Cytolytic activity
PerCP/Cy5.5 anti-mouse CD107a	1D4B	Biolegend	Degranulation
PerCP/Cy5.5 anti-mouse Ki-67	16A8	Biolegend	Proliferation
PE/Cy7 anti-mouse CD3ε	145-2C11	Biolegend	T cell
PE/Cy7 anti-mouse/human CD11b	M1/79	Biolegend	Myeloid cells
Purified anti-mouse CD16/32	93	Biolegend	Blockade of FcγRs
FITC anti-rat His48	HIS48	eBioscience	Rat granulocyte
PE anti-rat CD11b/c	OX42	eBioscience	Rat macrophages, monocyte, granulocytes, and dendritic cells
MACS Sorting			
Biotin anti-mouse Ly-6G/Ly-6C (Gr-1)	RB6-8C5	Biolegend	Mouse MDSCs
Biotin anti-rat His 48	HIS48	ThermoFisher Scientific	Rat MDSCs
Biotin anti-rat CD11b/c	OX42	Biolegend	Rat macrophages, monocyte, granulocytes, and dendritic cells

References:

(1) Kim, J.; Lee, Y.M.; Kang, Y.; Kim, W. J. Tumor-Homing, Size-Tunable Clustered Nanoparticles for Anticancer Therapeutics. *ACS Nano* **2014**, *8* (9), 9358–9367. https://doi.org/10.1021/nn503349g.

(2) Ingo P Korndörfer, Florian Brueckner, A. S. The Crystal Structure of the Human (S100A8/S100A9) 2 Heterotetramer, Calprotectin, Illustrates How Conformational Changes of Interacting α-Helices Can Determine Specific Association of Two EF-Hand Proteins. *J. Mol. Biol.* **2007**, *370* (5), 887–898. https://doi.org/10.1016/j.jmb.2007.04.065.

(3) William L. Jorgensen, Jayaraman Chandrasekhar, J. D. M. Comparison of Simple Potential Functions for Simulating Liquid Water. *J Chem Phys* **1983**, *79*, 926–935. https://doi.org/doi.org/10.1063/1.445869.

(4) William Humphrey, Andrew Dalke, K. S. VMD: Visual Molecular Dynamics. *J Mol Graph* **1996**, *14*, 33–38. https://doi.org/10.1016/0263-7855(96)00018-5.

(5) Jing Huang, Sarah Rauscher, Grzegorz Nawrocki, Ting Ran, Michael Feig, Bert L de Groot, H. G. & A. D. M. J. CHARMM36m: An Improved Force Field for Folded and Intrinsically Disordered Proteins. *Nat. Methods* **2017**, *14* (1), 71–73. https://doi.org/10.1038/nmeth.4067.

(6) Vanommeslaeghe K, Hatcher E, Acharya C, Kundu S, Zhong S, Shim J, Darian E, Guvench O, Lopes P, Vorobyov I, M. A. J. CHARMM General Force Field: A Force Field for Drug- like Molecules Compatible with the

CHARMM All- atom Additive Biological Force Fields. Journal of Computational Chemistry. *J Comput Chem.* **2010**, *31* (4), 671–690. https://doi.org/10.1002/jcc.21367.

(7) Rebecca S. Bamert, Karl Lundquist, Hyea Hwang, Chaille T. Webb, Takoya Shiota, Christopher J. Stubenrauch, Mathew J. Belousoff, Robert J. A. Goode, Ralf B. Schittenhelm, Richard Zimmerman, Martin Jung, James C. Gumbart, and T. L. Structural Basis for Substrate Selection by the Translocation and Assembly Module of the B- barrel Assembly Machinery. *Mol. Microbiol.* **2017**, *106* (1), 142–156. https://doi.org/10.1111/mmi.13757.

(8) Martyna GJ, Tobias DJ, K. M. Constant Pressure Molecular Dynamics Algorithms. *J Chem Phys* **1994**, *101*, 4177–4189. https://doi.org/doi.org/10.1063/1.467468.

(9) Darden T, York D, P. L. Particle Mesh Ewald: An N· Log (N) Method for Ewald Sums in Large Systems. *J. Chem. Phys.* **1993**, *98* (12), 10089–10092. https://doi.org/doi.org/10.1063/1.464397.

(10) Phillips JC, Braun R, Wang W, Gumbart J, Tajkhorshid E, Villa E, Chipot C, Skeel RD, Kalé L, S. K. Scalable Molecular Dynamics with NAMD. *J Comput Chem* **2005**, *26* (16), 1781–1802. https://doi.org/10.1002/jcc.20289.

(11) D.A. Case, R.M. Betz, D.S. Cerutti, T.E. Cheatham, III, T.A. Darden, R.E. Duke, T.J. Giese, H. G.; A.W. Goetz, N. Homeyer, S. Izadi, P. Janowski, J. Kaus, A. Kovalenko, T.S. Lee, S. LeGrand, P. Li, C.; Lin, T. Luchko, R. Luo, B. Madej, D. Mermelstein, K.M. Merz, G. Monard, H. Nguyen, H.T.

Nguyen, I.; Omelyan, A. Onufriev, D.R. Roe, A. Roitberg, C. Sagui, C.L. Simmerling, W.M. Botello-Smith, J. S.; R.C. Walker, J. Wang, R.M. Wolf, X. Wu, L. X. and P. A. K. *AMBER 2016*; University of California, San Francisco, 2016.

(12) Chad W. Hopkins, Scott Le Grand, Ross C. Walker, A. E. R. Long-Time-Step Molecular Dynamics through Hydrogen Mass Repartitioning. *J. Chem. Theory Comput.* **2015**, *11* (4), 1864–1874. https://doi.org/10.1021/ct5010406.

(13) Curtis Balusek, Hyea Hwang, Chun Hon Lau, Karl Lundquist, Anthony Hazel, Anna Pavlova, Diane L. Lynch, Patricia H. Reggio, Yi Wang, J. C. G. Accelerating Membrane Simulations with Hydrogen Mass Repartitioning. *J. Chem. Theory Comput.* **2019**, *15* (8), 4673–4686. https://doi.org/10.1021/acs.jctc.9b00160.

(14) Donnelly, E. M.; Kubelick, K. P.; Dumani, D. S.; Emelianov, S. Y. Photoacoustic Image-Guided Delivery of Plasmonic-Nanoparticle-Labeled Mesenchymal Stem Cells to the Spinal Cord. *Nano Lett.* **2018**, *18* (10), 6625–6632. https://doi.org/10.1021/acs.nanolett.8b03305.